Cholinergic input to mouse visual cortex signals a movement state and acutely enhances layer 5 responsiveness

Baba Yogesh[1,2] & Georg B. Keller[1,2,3]

[1]*Friedrich Miescher Institute for Biomedical Research, Basel, Switzerland.*
[2]*Faculty of Natural Sciences, University of Basel, Basel, Switzerland.*
[3]*Correspondence to: georg.keller@fmi.ch*

ABSTRACT

Acetylcholine is released in visual cortex by axonal projections from the basal forebrain. The signals conveyed by these projections and their computational significance are still unclear. Using two-photon calcium imaging in behaving mice, we show that basal forebrain cholinergic axons in the mouse visual cortex provide a binary locomotion state signal. In these axons, we found no evidence of responses to visual stimuli or visuomotor prediction errors. While optogenetic activation of cholinergic axons in visual cortex in isolation did not drive local neuronal activity, when paired with visuomotor stimuli, it resulted in layer-specific increases of neuronal activity. Responses in layer 5 neurons to both top-down and bottom-up inputs were increased in amplitude and decreased in latency, whereas those in layer 2/3 neurons remained unchanged. Using opto- and chemogenetic manipulations of cholinergic activity, we found acetylcholine to underlie the locomotion-associated decorrelation of activity between neurons in both layer 2/3 and layer 5. Our results suggest that acetylcholine augments the responsiveness of layer 5 neurons to inputs from outside of the local network, possibly enabling faster switching between internal representations during locomotion.

**** Dear reader, please note this manuscript is formatted in a standard submission format, and all statistical information is in Table S1. ****

INTRODUCTION

Acetylcholine is one of the key neuromodulators involved in cortical function and plasticity. A rich body of work has shown that acetylcholine gates experience-dependent changes in the responses of cortical neurons to sensory inputs. This includes receptive field plasticity in auditory cortex (Bakin et al., 2012; Froemke et al., 2007; Kilgard and Merzenich, 1998; Metherate and Weinberger, 1990), somatosensory

cortex (Ego-Stengel et al., 2001; Rasmusson and Dykes, 1988; Sachdev et al., 1998), and olfactory cortex (Wilson et al., 2004), or ocular dominance plasticity in visual cortex (Bear and Singer, 1986; Greuel et al., 1988; Gu and Singer, 1993; Kirkwood et al., 1999). In all cases, the central tenet is that pairing of acetylcholine release or its application concurrent with a sensory stimulus results in plasticity that increases the responsiveness of neurons to subsequent presentations of the same stimulus. While the evidence that acetylcholine gates plasticity is overwhelming and unequivocal, it remains less well understood what drives the release of acetylcholine in cortex during behavior and what its functional consequences are on cortical computations acutely.

Cholinergic projections to cortex arise from a population of neurons in the basal forebrain (Li et al., 2018). Within this population of neurons, there is a relatively broad functional heterogeneity (Laszlovszky et al., 2020; Robert et al., 2021), with responses observed during movement – be it locomotion or licking (Harrison et al., 2016), to reinforcers (Hangya et al., 2015), to auditory stimuli (Guo et al., 2019; Robert et al., 2021), and weakly to visual stimuli (Robert et al., 2021). However, inferring acetylcholine release in specific cortical targets based on activity of cholinergic neurons within the basal forebrain is complicated by the fact that different regions (Kim et al., 2016; Pinto et al., 2013) and cholinergic cell types (Laszlovszky et al., 2020) in the basal forebrain project to different areas of cortex. This projection specificity likely underlies the heterogeneity in cholinergic activity across dorsal cortex (Collins et al., 2023; Lohani et al., 2022). Measurements of cholinergic activity in cortex have found that movement in the form of a lever press is associated with cholinergic activity in mouse motor cortex, somatosensory cortex, and prefrontal cortex (Ren et al., 2022). Whisking is associated with cholinergic axonal activity in barrel cortex (Eggermann et al., 2014), while sound (Zhu et al., 2023) and movement (Nelson and Mooney, 2016; Zhu et al., 2023) are associated with cholinergic activity in auditory cortex, and locomotion (Larsen et al., 2018; Lohani et al., 2022), facial movement (Lohani et al., 2022), and pupil dilation (Larsen et al., 2018; Reimer et al., 2016) are associated with cholinergic activity in visual cortex. Overall, cholinergic activity in cortex is closely related to movement, but whether movement is the primary determinant of cholinergic activity and how movement related activity compares to sensory driven activity is less clear.

Likely the primary functional effect of increased levels of acetylcholine in cortex is increased sensory responsiveness. Local application of acetylcholine has been shown to increase sensory responses in somatosensory cortex (Chatfield and Dempsey, 1941), auditory cortex (Forster and McCarter, 1946), as well as visual cortex (Sato et al., 1987) in anesthetized cats. A similar gain in visually evoked responses in rodent visual cortex can be induced by iontophoretic application of acetylcholine in cortex (Sillito and

Kemp, 1983), by systemic acetylcholine release following basal forebrain stimulation (Goard and Dan, 2009; Pafundo et al., 2016), or by optogenetic stimulation of basal forebrain cholinergic axons in visual cortex (Pinto et al., 2013). Interestingly, this increase of sensory responses caused by acetylcholine is not homogeneous across cortical layers. Neurons responsive to iontophoretic application of acetylcholine are preferentially found in deep cortical layers (Krnjević and Phillis, 1963). The effects of acetylcholine are primarily one of facilitation of neuronal responses in deep cortical layers and one of suppression in superficial layers (Sillito and Kemp, 1983; Soma et al., 2013). However, depending on how locally acetylcholine is applied, it can also result in selective hyperpolarization of layer 5 neurons (Gulledge et al., 2007). Triggering systemic increase of acetylcholine by nucleus basalis stimulation results in firing rate increases in layers 4, 5, and 6 of visual cortex, but decreased firing rates in layer 2/3 (Goard and Dan, 2009). While it is unclear whether the effect observed in the experiments that use systemic modulation of cholinergic activity is cortical or reflects a combination of changes in subcortical and cortical processing, a direct layer-specific effect on cortical processing would be consistent with differential expression of acetylcholine receptors across cortical layers (Obermayer et al., 2017). Based on these findings it is often assumed that the local release of acetylcholine in cortex differentially influences deep and superficial cortical layers.

A second functional effect of acetylcholine is a decorrelation of cortical activity. Both basal forebrain cholinergic neuron stimulation and local cholinergic axon stimulation in visual cortex desynchronizes activity in visual cortex (Pinto et al., 2013). This effect is thought to be mediated by the influence of acetylcholine on somatostatin positive interneurons and their interaction with the excitatory neurons. This is based on the finding that optogenetic inhibition of somatostatin interneurons blocks acetylcholine induced decorrelation (Chen et al., 2015), and that optogenetically induced acetylcholine release selectively enhances the input from excitatory neurons onto somatostatin interneurons (Urban-Ciecko et al., 2018). A similar decrease in correlation has also been observed during locomotion (Aydın et al., 2018; Erisken et al., 2014), and the effect was stronger in deeper layers of cortex (Dadarlat and Stryker, 2017). It is possible that the decrease of correlations observed during locomotion is driven by locomotion related increases in acetylcholine.

More generally, following the discovery of the modulation of sensory evoked responses by locomotion in visual cortex (Niell and Stryker, 2010), it has been speculated that acetylcholine is involved in locomotion related changes in neuronal activity. Based on studies in rodents, a circuit was delineated that projects from mesencephalic locomotor region to the basal forebrain, which when active, can bring about a gain

91 of responses in visual cortex to visual stimuli (Lee et al., 2014). It has been argued that nicotinic activation
92 of vasoactive intestinal peptide (VIP) expressing interneurons in visual cortex is necessary for this
93 locomotion induced gain of visual responses (Fu et al., 2014). While VIP interneurons are clearly
94 influenced by acetylcholine (Gasselin et al., 2021), cholinergic receptors are expressed in all cortical cell
95 types (Colangelo et al., 2019), and there are likely direct functional effects of acetylcholine on many other
96 cell types (Alitto and Dan, 2012; Chen et al., 2015; Gulledge and Stuart, 2005; Hay et al., 2016; Hedrick
97 and Waters, 2015; Unal et al., 2012; Xiang, 1998; Zolles et al., 2009). This has called into question the
98 interpretation that acetylcholine is involved in locomotion related changes in neuronal activity primarily
99 through nicotinic activation of VIP neurons - it is more likely that most cortical cell types are directly
100 influenced (Pakan et al., 2016). The specific subtypes of muscarinic and nicotinic receptors expressed
101 across these different cell types further complicate causal attribution of effects. Nevertheless, all these
102 lines of evidence come together to suggest that basal forebrain cholinergic axons in visual cortex increase
103 their activity on locomotion and release acetylcholine to bring about a gain of visually evoked responses.
104 Throughout the manuscript, we will refer to basal forebrain cholinergic axons simply as cholinergic axons.
105 This distinction notably excludes potential axons that arise from local VIP-ChAT$^+$ neurons (Granger et al.,
106 2020), that are labeled when using a cross of ChAT-Cre mice with a reporter line. Prior measurements of
107 the activity of cholinergic axons in visual cortex all either have relied on data from a cross of ChAT-Cre
108 mice with a reporter line (Larsen et al., 2018; Reimer et al., 2016), which result in co-labelling of local VIP-
109 ChAT$^+$ neurons, or have pooled imaging data across cortical regions (Collins et al., 2023), which obscures
110 the projection-specificity of basal forebrain cholinergic axons to cortex (Kim et al., 2016). Thus, it remains
111 unclear what the response profile of cholinergic axons in mouse visual cortex is and what the functional
112 role of this input may be.

113 In this work, we sought to understand the signals conveyed by the basal forebrain cholinergic system to
114 visual cortex, the consequent changes to activity of layer 2/3 and layer 5 neurons in visual cortex upon
115 release of acetylcholine, and the potential implications this could have on the computations performed
116 by visual cortex. We used two-photon calcium imaging of cholinergic axons in visual cortex in behaving
117 head-fixed mice and found that cholinergic activity in visual cortex was best approximated as a locomotion
118 state signal. The effects of optogenetic activation of cholinergic axons locally in visual cortex were layer-
119 specific: the responsiveness was increased in neurons in layer 5 but not in layer 2/3. Furthermore, we
120 provide evidence that acetylcholine release underlies the locomotion related decorrelation of activity in
121 visual cortex.

RESULTS

To investigate the function of cholinergic input to visual cortex, we first characterized the calcium activity in these axons. We used an AAV vector to express an axon-targeted GCaMP6s (Broussard et al., 2018) in basal forebrain cholinergic neurons using ChAT-IRES-Cre mice (Rossi et al., 2011) and recorded calcium activity of their axons in visual cortex using two-photon microscopy (**Figures 1A and 1B**). For imaging experiments, mice were head-fixed on a spherical treadmill surrounded by a toroidal screen (**Figure 1C**). We used a set of different visuomotor conditions known to activate neurons in visual cortex to probe for activation of cholinergic axons. First, mice were exposed to a closed loop condition during which locomotion velocity was coupled to movement in a virtual tunnel. We then measured activity in an open loop condition during which locomotion and movement in the virtual tunnel were uncoupled, in darkness, and during presentation of full field drifting gratings. Throughout all experimental conditions mice were free to locomote on the spherical treadmill and did so over a range of velocities (**Video S1**).

We found that the activity in many cholinergic axons strongly increased during locomotion (**Figures 1D and 1E**). Activity increased with locomotion onset (**Figure 1F**) with an average lag across all responsive axons of 477 ms relative to locomotion onset (**Figure S1A**). Thus, consistent with results reported for auditory cortex (Nelson and Mooney, 2016), we found that locomotion preceded the increase in cholinergic activity in visual cortex. Locomotion onset also results in an increase in activity of neurons in primary visual cortex (Ayaz et al., 2013; Keller et al., 2012; Saleem et al., 2013). It has been speculated that cholinergic input is a driver of locomotion related activity in visual cortex (Lee et al., 2014). We thus compared the observed response latency between cholinergic input and activity of layer 2/3 and layer 5 neurons. The response latency of cholinergic axons was longer than the latency we observed in responses of layer 2/3 neurons (**Figure S1B**), but shorter than that of layer 5 neurons (**Figures S1C and S1D**). This would suggest that the initial increase in neuronal activity in layer 2/3 of the visual cortex was not driven by cholinergic input from basal forebrain.

Interestingly, we found no evidence of a response of cholinergic axons to other stimuli that drive responses in visual cortex such as full field drifting gratings (**Figure 1G**), visual flow onsets in open loop (**Figure 1H**), or visuomotor mismatches (**Figure 1I**) (Attinger et al., 2017; Jordan and Keller, 2020; Keller et al., 2012; Niell and Stryker, 2008; Vasilevskaya et al., 2023; Widmer et al., 2022). Visuomotor mismatches are brief visual flow halts that break the coupling between locomotion and visual flow feedback in a closed loop condition. Consistent with the absence of response to visual stimuli – full field drifting gratings or visual flow in open loop, we found that the response to locomotion onset was independent of whether

153 the locomotion occurred in darkness, in the presence of visual stimuli, or with visual flow feedback
154 coupled to locomotion (**Figure 1J**). For each imaging site, we then quantified the percentage of cholinergic
155 axons that exhibited significant responses to locomotion onset, full field drifting gratings, or visuomotor
156 mismatch, and found that 52.3% ± 4.4% (mean ± SEM) of the axons responded significantly to locomotion
157 onset, while the fraction of responsive axons to gratings and mismatch was not different from chance
158 (**Figure 1K**).

159 To confirm that an increase in calcium activity in cholinergic axons corresponds to an increase in
160 extracellular acetylcholine, we measured acetylcholine levels using the genetically-encoded acetylcholine
161 sensor GRAB-Ach3.0 (Jing et al., 2020). The sensor was expressed in visual cortex, and we performed two-
162 photon imaging in layer 2/3 during the same visuomotor conditions as described above. We found that
163 consistent with the calcium activity of cholinergic axons, acetylcholine levels in visual cortex increased on
164 locomotion onsets (**Figure S2A**), while grating onsets (**Figure S2B**) and visuomotor mismatches (**Figure**
165 **S2C**) resulted in no measurable increase when corrected for hemodynamic artifacts (**Figures S2A-S2F**).
166 Thus, consistent with previous reports (Larsen et al., 2018), we find that locomotion is associated with a
167 basal forebrain driven increase in acetylcholine levels in visual cortex.

168 Further characterizing the relationship between locomotion velocity and cholinergic activity, we found
169 that cholinergic axon activity was not linearly related to locomotion velocity, but instead exhibited a
170 locomotion state dependence. Over the course of a locomotion bout, we found that velocity decreased
171 systematically, such that towards the end of a locomotion bout, velocity was lower than at the beginning
172 (**Figure 2A**). For cholinergic activity, this decrease was absent. We found no evidence of a difference in
173 the average calcium activity of cholinergic axons after locomotion onset to that before locomotion offset
174 (**Figure 2B**). Indeed, the average cholinergic activity after locomotion onset and before locomotion offset
175 was highly correlated across locomotion bouts, while a similar analysis on locomotion velocity revealed
176 that the time-course of velocity is more variable and less correlated bout-by-bout (**Figure 2C**). The
177 similarity of locomotion onset and offset responses was not only true for the population average activity,
178 but the activity after locomotion onset, before locomotion offset, and the average activity during the
179 locomotion bout were all well correlated on an axon-by-axon level (**Figures 2D and S2G**). To quantify the
180 relationship between locomotion velocity and calcium activity in cholinergic axons more generally, we
181 computed the average calcium activity as a function of locomotion velocity (see Methods). This
182 relationship was more step-like than linear, and we found no evidence of an increase in calcium activity
183 between low and high locomotion velocities (**Figure 2E**). The same held true for extracellular acetylcholine

levels as measured by GRAB-ACh3.0 (**Figure S2H**). If calcium activity in cholinergic axons reflected a step-like change during locomotion, we should find that calcium activity correlates better with a binarized version of locomotion velocity than with locomotion velocity itself. This is indeed what we found (**Figure 2F**), independent of the value of the threshold used for binarization (**Figure S3**). Thus, calcium activity in cholinergic axons in visual cortex is better described as a binary locomotion state signal, than a linear locomotion velocity signal.

A number of behavioral variables, like pupil dilation, facial movements, as well as the overall level of arousal are all correlated with locomotion (Lohani et al., 2022; Reimer et al., 2014; Vinck et al., 2015). It has been shown that cholinergic activity in visual cortex is also well correlated with pupil dilation and facial movements (Larsen et al., 2018; Lohani et al., 2022; Reimer et al., 2014). Disambiguating the effects of locomotion, pupil dilation, and intensity of facial movements on cholinergic activity is complicated by the fact that these three variables are strongly correlated during behavior. It has been shown that under certain conditions, facial movements are a better predictor of cholinergic activity than locomotion across large parts of dorsal cortex (Lohani et al., 2022). To quantify this relationship in visual cortex, we compared the correlation between cholinergic activity, locomotion velocity, pupil diameter, and intensity of facial movements in different visuomotor conditions. This analysis was motivated by our observation that average light levels have a stronger influence on pupil size than locomotion state. We found that the correlation of locomotion velocity and cholinergic activity was independent of visuomotor condition (**Figure 3A**). This was not the case for the correlation between pupil diameter and cholinergic activity, which was systematically lower in darkness than in conditions with visual stimuli, and lower during closed loop visuomotor coupling than during open loop or grating conditions (**Figure 3B**). This pattern was also reflected in the correlation between locomotion and pupil diameter (**Figure 3C**). The reduced correlation between locomotion velocity and pupil diameter in darkness was not a consequence of a decrease in variability due to ceiling-effects in pupil diameter in darkness (**Figure S4A**). Finally, we also computed the correlation between cholinergic activity and facial movements. The correlation of cholinergic activity with locomotion was higher than that with facial movements under all conditions that we tested (**Figure S4B**). Thus, of these three behavioral variables, locomotion, pupil diameter, and facial movements, locomotion exhibited the most robust correlation with cholinergic activity in visual cortex (**Figure S4C**).

Next, we turned to the question of what the influence of increased cholinergic activity in visual cortex is on the activity of neurons in layer 2/3 and layer 5. We know that locomotion influences neuronal activity in visual cortex in a variety of ways. One of these effects is that during locomotion, visual responses in

visual cortex are increased (Niell and Stryker, 2010) through a combination of both additive and multiplicative effects (Dadarlat and Stryker, 2017). Consistent with this we found locomotion driven increases in visual responses were apparent in both layer 2/3 (**Figure 4A**) and in layer 5 neurons (**Figure 4B**). To test whether this increase in visual responsiveness during locomotion was driven by acetylcholine, we expressed the excitatory opsin ChrimsonR (Klapoetke et al., 2014) in basal forebrain cholinergic neurons using an AAV2/1-hSyn-DIO-ChrimsonR-tdTomato vector in ChAT-IRES-Cre mice. We injected an AAV2/1-Ef1α-GCaMP6f in visual cortex to express GCaMP6f. In cortex, the Ef1α promoter drives highly specific expression in neurons (99.7% of labeled cells in layer 2/3 and 100% of labeled cells in layer 5 are NeuN-positive (Yaguchi et al., 2013)), and biases expression to excitatory neurons, such that approximately 95% of labeled neurons are excitatory in both layer 2/3 (Attinger et al., 2017; Yaguchi et al., 2013) and in layer 5 (Yaguchi et al., 2013). We then performed two-photon calcium imaging in visual cortex to measure the responses of layer 2/3 or layer 5 neurons to the optogenetic activation of local cholinergic axons paired to the presentation of full field drifting grating stimuli while the mouse was stationary (see Methods). We found that in layer 2/3, optogenetic activation of cholinergic axons did not result in a detectable increase in grating onset responses (**Figures 4C and S6A**), while the responses of layer 5 neurons to the same stimulus increased with concurrent optogenetic activation of cholinergic axons (**Figure 4D**). The effects of optogenetic activation of cholinergic axons on layer 5 neurons could not be explained by a stimulation triggered change in locomotion velocity (**Figure S5**) or stimulation artifacts (**Figures S7A-S7C**). In mice that did not express ChrimsonR in cholinergic axons (no ChrimsonR controls), we found no evidence of an optogenetic light stimulation effect. Interestingly, this increase in grating onset responses in layer 5 neurons driven by direct cholinergic activation was smaller than that observed during locomotion (**Figures 4B and 4D**). This could be either because the acetylcholine release triggered by the optogenetic stimulation of cholinergic axons was weaker than that occurring during locomotion, or because the increase in responses during locomotion is only partially explained by the co-release of acetylcholine. If the former were the case, we would expect that responses occurring during locomotion are less influenced by optogenetic activation of cholinergic axons. This was indeed the case for grating onset responses during locomotion which were not modulated by optogenetic activation of cholinergic axons (**Figures S7D and S7E**). Interestingly, visuomotor mismatch responses, which also occur only during locomotion, were significantly increased in layer 5 neurons (**Figure 4F**), but not in layer 2/3 (**Figures 4E and S6B**). Similarly, we found that optogenetic activation of cholinergic axons increased locomotion onset responses in layer 5 neurons (**Figure 4H**), while layer 2/3 neurons exhibited no significant difference (**Figures 4G and S6C**). Thus, while in layer 5 neurons the effect of optogenetic activation appears to

247 saturate for bottom-up grating responses during locomotion, this was not the case for responses that rely
248 on top-down input. However, it is also likely that the increase in response during locomotion is only
249 partially explained by acetylcholine. Locomotion has been shown to result in both a multiplicative and an
250 additive change in grating responses (Dadarlat and Stryker, 2017). This was also the case in our data for
251 locomotion related increase in grating responses (**Figure S8**). However, we found that the optogenetic
252 stimulation of cholinergic axons resulted primarily in a multiplicative gain of visual responses (**Figure S8**).
253 Overall, consistent with previous findings (Goard and Dan, 2009), we find that acetylcholine primarily
254 increases both bottom-up and top-down driven responses in layer 5 but not layer 2/3 neurons, but only
255 partially explains the locomotion driven increases in visual responses.

256 A second effect of locomotion on neuronal activity in visual cortex is that locomotion itself drives neuronal
257 responses (Keller et al., 2012; Saleem et al., 2013). This effect is apparent in both layer 2/3 (**Figure 5A**)
258 and layer 5 (**Figure 5B**) neurons. In layer 2/3, locomotion related activity is suppressed by closed loop
259 visual feedback (Widmer et al., 2022), as a function of the strength of visuomotor mismatch responses
260 (**Figure S9A and S9B**). In layer 5, closed loop visual feedback did not suppress running related activity on
261 average in either visuomotor mismatch or grating responsive neurons (**Figure S9C and S9D**). Thus,
262 locomotion related activity likely has functionally distinct roles in layer 2/3 and layer 5. To test whether
263 artificial activation of cholinergic axons would result in increased neuronal activity, we again performed
264 two-photon calcium imaging in visual cortex neurons to measure responses of layer 2/3 or layer 5 neurons
265 upon optogenetic activation of local cholinergic axons. We found no evidence of any increase in calcium
266 activity in either layer 2/3 (**Figure 5C**) or layer 5 neurons (**Figure 5D**). This absence of a stimulation
267 response is consistent with previous reports that found that cholinergic axon stimulation in visual cortex
268 does not result in a response of layer 2/3 neurons (Chen et al., 2015) and that electrical stimulation of
269 basal forebrain primarily activates inhibitory neurons in superficial layers of visual cortex (Alitto and Dan,
270 2012). This, combined with our finding that on average the layer 2/3 locomotion onset related activity
271 preceded the activity increase in cholinergic axons (**Figure S1**), would indicate that the locomotion related
272 increase in layer 2/3 and layer 5 activity observed in visual cortex is not driven by acetylcholine.

273 A third effect locomotion has on neuronal activity in visual cortex is to decorrelate the activity of nearby
274 neurons (Dadarlat and Stryker, 2017; Erisken et al., 2014). Consistent with these studies, we found that
275 locomotion results in a reduction of pairwise correlations between activity of layer 2/3 neurons (**Figures**
276 **6A and 6E**) as well as between layer 5 neurons (**Figures 6B and 6F**). We could induce this decorrelation by
277 optogenetically activating the cholinergic axons while mice were stationary. This optogenetically induced

278 decorrelation in layer 2/3 (**Figures 6C and 6E**) was stronger than that driven by locomotion, while the two
279 were similar in layer 5 (**Figures 6D and 6F**). Note, we used calcium activity of apical dendrites of L5 neurons
280 in L2/3 as a proxy for somatic L5 activity in these experiments (see Methods). This decorrelation was not
281 due to a visual response to the stimulation laser (**Figure S7F**). Interestingly, we found that in both layer
282 2/3 and layer 5, the locomotion induced decorrelation was observed primarily for neurons with low
283 pairwise correlations. Pairs of neurons with high correlation of activity tended to further increase their
284 correlation during locomotion (**Figure S10**). Finally, we tested whether the correlation in visual cortex was
285 similarly influenced by chemogenetic manipulation of basal forebrain cholinergic neurons. We expressed
286 either a DREADD activator or a DREADD inhibitor in ChAT-Cre mice to systemically increase or decrease
287 cholinergic activity. Interestingly, we noticed that the systemic increase or decrease of cholinergic release
288 resulted in behavioral changes in the mice. Upon chemogenetic activation mice increased their
289 locomotion velocity, and upon chemogenetic inhibition, mice decreased their time spent locomoting,
290 resulting in a bidirectional modulation of the total distance traveled by the two manipulations (**Figure**
291 **S11**). Importantly, chemogenetic manipulations bidirectionally modulated the decorrelation effect on
292 locomotion in layer 5 neurons in visual cortex. DREADD activation resulted in an increased strength of the
293 locomotion driven decorrelation, while DREADD inhibition resulted in a reduced strength of locomotion
294 driven decorrelation in layer 5 (**Figures 6H and S12B**). This effect was absent in layer 2/3 where neither
295 manipulation influenced the locomotion driven decorrelation (**Figures 6G and S12A**). Thus, cholinergic
296 activation is likely sufficient to explain the locomotion induced decorrelation of activity in visual cortex.

297 Finally, an effect of locomotion on the responses of layer 5 neurons, which to the best of our knowledge
298 is unreported, is a decrease in latency to response. In layer 5 neurons, responses to grating stimuli
299 appeared earlier during locomotion than they did while the mouse was stationary (**Figures 4B and 7B**).
300 This decrease in response latency during locomotion was absent in layer 2/3 neurons (**Figures 4A and 7A**).
301 Optogenetic activation of cholinergic axons was able to recapitulate the decrease in response latency in
302 layer 5 neurons (**Figures 4D, 7B and S13B**), while leaving layer 2/3 neuron response latency unaffected
303 (**Figures 4C, 7A and S13A**). Thus, cholinergic input decreases the response latency of layer 5 neurons.

304 DISCUSSION

305 We set out to address the question of why acetylcholine is released in visual cortex by answering two
306 simpler, intermediate questions: what drives acetylcholine release, and what immediate effects does the
307 released acetylcholine have on the cortical circuits. We found that locomotion was the main driver of

308 ChAT axons activity (**Figure 1**) and acetylcholine release (**Figure S2**) in visual cortex, and cholinergic activity
309 depended on locomotion velocity in a non-linear, step-like manner (**Figure 2**). The acute effects of this
310 increase in acetylcholine on cortical responses were layer-specific: acetylcholine release enhanced
311 responses specifically in layer 5 neurons, but not in layer 2/3 (**Figure 4**). Using chemogenetic
312 manipulations of basal forebrain cholinergic neurons, we found that we could bidirectionally influence
313 the activity correlations of layer 5 neurons. Cholinergic activation resulted in a decrease of pairwise
314 correlations while inhibition resulted in an increase (**Figure 6H**). We observed a similar decrease in
315 pairwise correlations during optogenetic stimulation of cholinergic axons in visual cortex, arguing that this
316 effect is, at least in part, mediated locally (**Figure 6F**). Similarly, optogenetic stimulation of cholinergic
317 axons in visual cortex drove a decrease in pairwise correlation of layer 2/3 (**Figure 6E**), while global
318 manipulation of the basal forebrain cholinergic system using chemogenetic tools did not significantly
319 change correlations on activation or inhibition (**Figure 6G**). Our results would be consistent with the
320 interpretation that the acute effects of acetylcholine are stronger in layer 5 where they act to increase
321 responsiveness to inputs from outside of the local layer 5 network.

322 While the optogenetic activation of cholinergic axons in visual cortex likely recapitulates the local effects
323 of acetylcholine more directly than those observed with basal forebrain stimulation, the method comes
324 with the following caveats. First, we don't know how the pattern of acetylcholine release induced by
325 optogenetic activation of cholinergic axons compares to that observed endogenously during locomotion.
326 The pattern of cholinergic axon activation was not uniform across axons (**Figures 1E and 2D**), consistent
327 with different modes of activity in cholinergic subpopulations observed in basal forebrain (Laszlovszky et
328 al., 2020). It is unclear whether the exact pattern of cholinergic axon activation substantially influences
329 the observed effects in cortex. However, given that the effects on changes in the correlation of activity
330 induced by optogenetic activation of cholinergic axons was at least as strong as that observed during
331 locomotion, we estimate that optogenetic activation of cholinergic axons can induce levels and patterns
332 of acetylcholine release similar to those observed endogenously. Second, the activation of cholinergic
333 axons likely antidromically activates cholinergic neuron soma in basal forebrain. Thus, we cannot exclude
334 the possibility of a systemic contribution to the effects we observe through shared projections between
335 different cortical and subcortical targets. However, the projection specificity of basal forebrain cholinergic
336 neurons (Kim et al., 2016; Pinto et al., 2013) would argue against this. Finally, it is important to note that
337 here we labeled basal forebrain cholinergic neurons with targeted viral injection. Thus, we cannot exclude
338 the possibility that our labelling of cholinergic axons was incomplete. The alternative approach to label
339 these neurons by crossing ChAT-Cre mice to a reporter line expressing a calcium indicator comes with the

340 caveat of the presence of a substantial fraction of VIP interneurons in visual cortex that also are ChAT
341 positive (Granger et al., 2020). Being unable to separate basal forebrain axons from those of local VIP
342 interneurons complicates the interpretation of results.

343 Another caveat of our conclusions is the fact that our neuronal populations in both layer 2/3 and layer 5
344 are not random subsets. While the Ef1α promoter is specific to neurons (Tsuchiya et al., 2002; Yaguchi et
345 al., 2013) and predominantly labels excitatory neurons (Attinger et al., 2017; Yaguchi et al., 2013), the
346 expression levels are likely not equal across the different excitatory neuron types. In layer 5, for example,
347 we are likely undersampling Tlx3-positive layer 5 neurons. Tlx3-positive layer 5 neurons exhibit a visually
348 driven reduction in activity and consequently have a systematic difference between open and closed loop
349 locomotion onsets (Heindorf and Keller, 2022). We do not see either a visually driven inhibition on average
350 (**Figure 4D**), nor a difference between closed and open loop locomotion onsets (**Figure S9**). Thus, it should
351 be kept in mind that with any virus based protein expression, the population of labeled cells is likely not
352 random genetically, and that descriptor of 'layer 2/3 (or 5) neuron' should be understood to mean, a 'layer
353 2/3 (or 5) neuron that exhibits high expression levels under the artificial Ef1α promoter when used in an
354 AAV delivery vector'.

355 Given our results, what are the implications for the computational role of acetylcholine in visual cortex?
356 There are likely two aspects to this, the acute effect on cortical activity and the effect on plasticity. We
357 find that acetylcholine was released in visual cortex as a locomotion state signal. This state signal could
358 be used to gate visuomotor plasticity. In systems engaged in sensorimotor learning, plasticity related to
359 feedback prediction errors should occur primarily during self-motion and not when passively experiencing
360 sensory input. Visuomotor development is critically dependent on coupling of locomotion and sensory
361 feedback (Attinger et al., 2017; Held and Hein, 1963; Kaneko and Stryker, 2014), and depends on local
362 plasticity mechanisms in visual cortex (Widmer et al., 2022). Acetylcholine is known to gate plasticity in
363 visual cortex (Bear and Singer, 1986; Greuel et al., 1988; Gu and Singer, 1993; Kirkwood et al., 1999) and
364 could function to gate visuomotor plasticity to phases of self-motion. Given that acetylcholine release is
365 associated with other types of movement as well (Eggermann et al., 2014; Harrison et al., 2016; Lohani et
366 al., 2022; Nelson and Mooney, 2016; Zhu et al., 2023), this is consistent with acetylcholine functioning
367 more generally as a movement state signal. We would predict that in visual cortex, this would primarily
368 relate to movements that result in changes to visual input.

369 The absence of an acute effect of optogenetically stimulating cholinergic axons locally on activity of visual
370 cortex neurons is consistent with the idea that locomotion driven neuronal activity in visual cortex (Keller

371 et al., 2012; Saleem et al., 2013) is likely not driven by acetylcholine, but is the consequence of a
372 combination of motor-related top-down input (Leinweber et al., 2017) and noradrenaline (Polack et al.,
373 2013), another neuromodulator that is known to accompany locomotion onset (Jordan and Keller, 2023;
374 Reimer et al., 2016). Consistent with previous reports (Goard and Dan, 2009), we find that acetylcholine
375 acutely increases visuomotor responses more strongly in layer 5 neurons than in layer 2/3 neurons and
376 that it decorrelates neuronal activity. One of the key questions here is why these effects are induced
377 during locomotion. There are a number of explanations that have been proposed previously that often
378 focus on increasing sensory gain to counteract the noisier visual input during locomotion (Minces et al.,
379 2017; Pinto et al., 2013). We propose a slightly more specific explanation. This is based on the idea that
380 the observed effects of acetylcholine on layer 5 can be explained by assuming the layer 5 network exhibits
381 attractor dynamics and that acetylcholine modifies these attractor dynamics (Kanamaru and Aihara,
382 2019). The observed differences in the effect of acetylcholine on layer 5, where response strength
383 increased, and layer 2/3, where they did not, are consistent with the interpretation that attractor
384 dynamics are stronger in layer 5 than in layer 2/3. This would, also agree with a proposed microcircuit for
385 predictive processing (Keller and Mrsic-Flogel, 2018), where layer 5 is postulated to maintain an internal
386 representation (Heindorf and Keller, 2022). Thus, acetylcholine could act to increase the sensitivity and
387 speed of response of the internal representation neurons to inputs arriving from outside the local network
388 at the expense of reducing the influence among neurons in the local network. Such an acetylcholine driven
389 increase in the speed of transition between different internal representations would also be consistent
390 with the finding that layer 5 neurons exhibit faster responses to the transitions between different stimuli
391 (**Figure 7**). Assuming the internal representation in cortex is a substrate of conscious perception, as
392 proposed by predictive processing, this would be consistent with the finding that anesthesia decouples
393 layer 5 neurons from their inputs onto apical dendrites by cholinergic mechanisms (Suzuki and Larkum,
394 2020).

395 What makes this hypothesis all the more tantalizing is the observation that a decrease in cortical
396 cholinergic activation is correlated with the severity of dementia in Alzheimer's disease (Perry et al., 1978).
397 All three drugs currently approved for the management of dementia in Alzheimer's disease are
398 cholinesterase inhibitors, drugs that increase acetylcholine levels. If cholinergic activation alters network
399 dynamics to make the putative layer 5 attractor network more sensitive to external inputs – and hence
400 more easily influenced by long-range cortical inputs – this could explain why cholinergic activation
401 enhances memory retrieval. A decrease in cholinergic tone in Alzheimer's disease is also consistent with
402 the increases of correlation of neuronal activity in cortex observed in mouse models of the disease

403 (Korzhova et al., 2021). Thus the cholinergic gating of the sensitivity of layer 5 to external inputs could
404 constitute a possible mechanism for the cholinergic hypothesis for Alzheimer's disease (Davies and
405 Maloney, 1976; Francis et al., 1999; Hampel et al., 2019; Terry and Buccafusco, 2003).

406 In summary, we show that cholinergic activity in visual cortex conveys a locomotion state signal, that
407 preferentially augments the response of layer 5 neurons to external inputs and decorrelates activity across
408 neurons, possibly to both sculpt the receptive field tuning of neurons to sensory stimuli as well as to
409 regulate the influence of external input on internal representation to affect our conscious percept.

410

411 # METHODS

412 ## Key Resources Table

REAGENT or RESOURCE	Source	Identifier
Bacteria and Virus Strains		
AAV2/5-hSyn1-FLEx-axon-GCaMP6s (10^{13}-10^{15} GC/ml)	FMI vector core	vector.fmi.ch
AAV PHP.eB-Ef1α-DIO-GCaMP6s (10^{11} GC/ml)	FMI vector core	vector.fmi.ch
AAV2/1-hSyn-DIO-ChrimsonR-tdTomato (10^{11}-10^{13} GC/ml)	FMI vector core	vector.fmi.ch
AAV2/1-Ef1α-GCaMP6f-WPRE (10^{11}-10^{14} GC/ml)	FMI vector core	vector.fmi.ch
AAV2/1-Ef1α-DIO-hM3D(Gq)-mCherry (10^{11} GC/ml)	FMI vector core	vector.fmi.ch
AAV2/1-Ef1α-DIO-hM4D(Gi)-mCherry (10^{11} GC/ml)	FMI vector core	vector.fmi.ch
AAV2/9-hSyn-GRAB-ACh3.0 (10^{13} GC/ml)	FMI vector core	vector.fmi.ch
AAV2/1-Ef1α-DIO-tdTomato-WPRE (10^{14} GC/ml)	FMI vector core	vector.fmi.ch
AAV2/1-Ef1α-GFP-WPRE (10^{12} GC/ml)	FMI vector core	vector.fmi.ch
Chemicals, Peptides, and Recombinant Proteins		
CNO	Tocris	Cat# 4936-10mg
Fentanyl citrate	Actavis	CAS 990-73-8
Midazolam (Dormicum)	Roche	CAS 59467-96-8
Medetomidine (Domitor)	Orion Pharma	CAS 86347-14-0
Ropivacaine	Presenius Kabi	CAS 132112-35-7
Lidocaine	Bichsel	CAS 137-58-6
Buprenorphine	Reckitt Benckiser Healthcare	CAS 52485-79-7
Ophthalmic gel (Humigel)	Virbac	-
Flumazenil (Anexate)	Roche	CAS 78755-81-4
Atipamezole (Antisedan)	Orion Pharma	CAS 104054-27-5
N-Butyl-2-cyanoacrylate (Histoacryl)	Braun	CAS 6606-65-1
Dental cement (Paladur)	Heraeus Kulzer	CAS 9066-86-8
Deposited data		
All data and code used to generate manuscript figures	This paper	data.fmi.ch
Experimental Models: Organisms/Strains		
Mus musculus: C57BL/6	Charles River	-
Mus musculus: B6J.129S6-Chat$^{tm2(Cre)Lowl}$/MwarJ	Jackson Laboratories	RRID:IMSR_JAX:028861
Software and algorithms		
MATLAB (2020b)	The MathWorks	RRID:SCR_001622
LabVIEW	National Instruments	RRID:SCR_014325
Two-photon acquisition software	Keller laboratory	sourceforge.net/p/iris-scanning/
Image data processing software	Keller laboratory	sourceforge.net/p/iris-scanning/calliope
Python	python.org	RRID:SCR_008394
Panda3D	panda3d.org	N/A
Other		

Virtual reality and two-photon setup	(Leinweber et al., 2014, 2017)	DOI: 10.3791/50885, 10.1016/j.neuron.2017.08.036
Optogenetic stimulation laser (OBIS 673 nm LX)	Coherent	Cat#1187194
Sham stimulation LED	Prizmatix	UHP-T-595
Titanium headplate	FMI/ETHZ workshop	N/A
Dental drill	Meisinger	N/A

413

414 **Mice.** All mice used in experiments described in the paper were ChAT-IRES-Cre (Rossi et al., 2011)
415 heterozygotes, kept on a C57BL/6 background. A total of 64 mice, both male and female, 6-16 weeks old
416 at the start of the experiment, were used. See **Table S2** for details of mouse inclusion for the different
417 figures. Between experiments, mice were group-housed in a vivarium (light/dark cycle: 12/12 hours). All
418 animal procedures were approved by and carried out in accordance with the guidelines laid by the
419 Veterinary Department of the Canton of Basel-Stadt, Switzerland.

420 **Surgery.** For all surgical procedures, mice were anesthetized with a mixture of fentanyl (0.05 mg/kg;
421 Actavis), midazolam (5.0 mg/kg; Dormicum, Roche), and medetomidine (0.5 mg/kg; Domitor, Orion)
422 injected intraperitoneally. Analgesics were applied perioperatively (2% lidocaine gel, meloxicam 5 mg/kg)
423 and postoperatively (buprenorphine 0.1 mg/kg, meloxicam 5 mg/kg). Eyes were covered with ophthalmic
424 gel (Virbac Schweiz AG). Cranial windows were implanted as previously described (Keller et al., 2012;
425 Leinweber et al., 2014). Briefly, using a dental drill, a 4 mm craniotomy was made over the right visual
426 cortex, centered 2.5 mm lateral and 0.5 mm anterior to lambda. After injection of AAV vectors, the
427 exposed cortex was sealed with a 4 mm circular glass coverslip and glued in place using gel superglue
428 (Ultra Gel, Pattex). The remaining exposed surface of the skull was covered with Histoacryl (B. Braun), and
429 a titanium head bar was fixed to the skull using dental cement (Paladur, Heraeus Kulzer). After surgery,
430 anesthesia was antagonized by a mixture of flumazenil (0.5 mg/kg; Anexate, Roche) and atipamezole (2.5
431 mg/kg; Antisedan, Orion Pharma) injected intraperitoneally.

432 **Axonal labeling.** To image the activity of basal forebrain cholinergic axons in visual cortex, we expressed
433 a calcium indicator in basal forebrain cholinergic neurons. Surgery was performed as described above,
434 and either an AAV2/5-hSyn1-FLEx-axon-GCaMP6s (10^{13} GC/ml) or an AAV-PHP.eB-Ef1α-DIO-GCaMP6s
435 (10^{12} GC/ml) was injected at four locations ipsilateral to the imaging site (AP, ML, DV (in mm): +1.1, +0.1,
436 -3.7 (medial septum); +1.1, +0.1, -4.1 and +0.8, +0.1, -4.2 (vertical limb of the diagonal band); +0.6, +0.6,
437 -4.9 (horizontal limb of the diagonal band)) in ChAT-IRES-Cre mice.

438 **GRAB imaging.** We injected an AAV vector carrying GRAB-ACh 3.0, AAV2/9-hSyn-GRAB-ACh3.0 (10^{13}
439 GC/ml), in visual cortex. A 4 mm craniotomy was made over right visual cortex and sealed with a glass
440 coverslip as described above.

441 **Chemogenetic experiments.** To manipulate the activity of the basal forebrain cholinergic system, we used
442 chemogenetic DREADD inhibitor AAV2/1-EF1α-DIO-hM4D(Gi)-mCherry (10^{11} GC/ml) or DREADD activator
443 AAV2/1-EF1α-DIO-hM3D(Gq)-mCherry (10^{11} GC/ml). AAVs were injected in anterior basal forebrain with
444 coordinates as used for axonal imaging described above. DREADDs were stimulated using Clozapine N-
445 oxide (CNO), which was dissolved in DMSO, diluted with saline, and injected intraperitoneally at a dose of
446 0.5 mg/kg body weight. Activity from each imaging site in the DREADD series was acquired starting 30 min
447 - 60 min after CNO injection.

448 **Optogenetic experiments.** We injected AAV2/1-hSyn-DIO-ChrimsonR-tdTomato (10^{11} GC/ml) into basal
449 forebrain at the same coordinates as for axonal imaging described above, and injected AAV2/1-Ef1α-
450 GCaMP6f-WPRE ($10^{11\text{-}14}$ GC/ml) into visual cortex for imaging neurons in layer 2/3 and layer 5. In no-opsin
451 control mice, instead of ChrimsonR, we injected an AAV2/1-DIO-tdTomato-WPRE (10^{14} GC/ml) virus.
452 ChrimsonR stimulation and functional imaging of GCaMP6f-expressing neurons was done as previously
453 described (Attinger et al., 2017). For imaging, we used a modified Thorlabs B-Scope with a 12 kHz
454 resonance scanner (Cambridge Technology). The illumination source for the optogenetic stimulation was
455 a 637nm laser (OBIS LX, Coherent). We used a dichroic mirror (ZT775sp-2p, Chroma) to combine the two-
456 photon laser and stimulation laser. A second long-pass dichroic mirror (F38-555SG, Semrock) was used to
457 split the GCaMP emission from both illumination light sources. Light leak from the 637 nm stimulation
458 laser was reduced by synchronizing the stimulation laser to the turnaround times of the resonant scanner
459 (during which imaging data were not acquired). Lastly, amplified PMT signals were digitally bandpass
460 filtered at 80 MHz to reduce the effect of ringing in the amplifier. This allowed for near stimulation-artifact
461 free synchronous imaging and optogenetic stimulation. For all experiments with stimulation of cholinergic
462 axons locally in visual cortex, we used a square-wave pulse of 1s duration and 10 mW/mm^2 power
463 (measured at objective). The median inter-trial interval for different stimulation events was 15 s for
464 optogenetic stimulation only trials, 12 s for optogenetic stimulation with grating onset, 35 s for
465 optogenetic stimulation with visuomotor mismatch, and 45 s for optogenetic stimulation with locomotion
466 onset in closed loop. To measure correlation changes, we employed a longer laser stimulation window of
467 1 minute, at 40 Hz (50% duty cycle), with an average power output of 20 mW/mm^2 (measured at

468 objective). For sham stimulation, we used an optical guide coupled to a high-power LED (UHP-T-595,
469 Prizmatix) to diffusely illuminate the mouse and surrounding virtual reality setup.

470 **Virtual reality environment.** The virtual reality setup is based on the design of Dombeck and colleagues
471 (Dombeck et al., 2007). Briefly, mice were head-fixed and free to run on an air-supported spherical
472 treadmill. The rotation of the ball was restricted around the vertical axis with a pin. The virtual reality
473 environment was projected onto a toroidal screen covering approximately 240 degrees horizontally and
474 100 degrees vertically of the mouse's visual field, using a projector (Samsung SP-F10M) synchronized to
475 the resonant scanner of the two-photon microscope. The virtual environment consisted of an infinite
476 corridor with walls patterned with vertical sinusoidal gratings with a spatial frequency of approximately
477 0.04 cycles per degree (Leinweber et al., 2014). In closed loop condition, the locomotion of the mouse
478 was coupled to movement along a virtual tunnel. In open loop condition, we uncoupled the two and
479 replayed the visual flow from a preceding closed loop condition. In grating condition, we presented full
480 field drifting gratings (0°, 45°, 90°, 270°, moving in either direction) in a pseudo-random sequence. Grating
481 stimuli were presented for between 2 s and 3 s. In the inter-stimulus interval (between 2 s and 4 s), mice
482 were shown a gray screen with average luminance matched to that of the grating stimuli.

483 **Eye tracking and facial movement measurement.** During all experiments, we recorded the mouse's left
484 eye (contralateral to the imaged hemisphere) with a CMOS infrared camera at 30 Hz frame rate. The pupil
485 was backlit by the 930 nm laser used for two-photon imaging. We calculated pupil diameter offline by
486 fitting a circle to the pupil. Frames with occluded pupil were excluded from analysis. To extract facial
487 movements, we computed the average image displacement in different image patches on the face of the
488 mouse.

489 **Two-photon microscopy.** Functional two-photon calcium imaging was performed using custom-built two-
490 photon microscopes (Leinweber et al., 2014). The illumination source was a tunable femtosecond laser
491 (Insight, Spectra Physics or Chameleon, Coherent) tuned to 930 nm. Emission light was band-pass filtered
492 using a 525/50 filter for GCaMP and a 607/70 filter for tdTomato/mCherry (Semrock) and detected using
493 a GaAsP photomultiplier (H7422, Hamamatsu). Photomultiplier signals were amplified (DHPCA-100,
494 Femto), digitized (NI5772, National Instruments) at 800 MHz, and band-pass filtered at 80 MHz using a
495 digital Fourier-transform filter implemented in custom-written software on an FPGA (NI5772, National
496 Instruments). The scanning system of the microscopes was based either on a 12 kHz or an 8 kHz resonant
497 scanner (Cambridge Technology). Images were acquired at a resolution of 750 x 400 pixels (60 Hz or 40
498 Hz frame rate, respectively), and a piezo-electric linear actuator (P-726, Physik Instrumente) was used to

499 move the objective (Nikon 16x, 0.8 NA) in steps of 15 µm between frames to acquire images at 4 different
500 depths. This resulted in an effective frame rate of 15 Hz or 10 Hz, respectively. The field of view was 375
501 µm x 300 µm.

502 **Extraction of neuronal activity.** Calcium imaging data were processed as previously described (Keller et
503 al., 2012) and all data analysis was done in MATLAB (MathWorks). Briefly, raw images were full-frame
504 registered to correct for lateral brain motion. Neurons and axons were manually selected based on mean
505 and maximum fluorescence images. For GRAB imaging, neuropil and blood vessels were manually
506 selected. For a subset of mice, the apical dendrites of layer 5 neurons were marked in layer 2/3 by
507 manually tracing them to their soma in layer 5 using a z-stack acquired at the end of an experiment. Raw
508 fluorescence traces were corrected for slow drift in fluorescence using an 8th-percentile filtering with a 66
509 s (or 1000 frames) window (Dombeck et al., 2007). ΔF/F traces were calculated as mean fluorescence in a
510 selected region of every imaging frame, subtracted and normalized by the overall median fluorescence.
511 All neuronal calcium activity data was acquired at 15 Hz. For axonal imaging, 9 (of 25 sites) were imaged
512 at 10 Hz, and analytically resampled at 15 Hz using a polyphase antialiasing filter to make the time-base
513 compatible with the rest of the axonal imaging data.

514 **Data analysis.** All data analysis was done using custom scripts written in MATLAB (MathWorks). To
515 quantify the average population response traces, we first calculated the average event-triggered
516 fluorescence trace for each region of interest (ROI). The responses of all ROIs was then averaged and
517 baseline-subtracted.

518 Locomotion onset was defined as locomotion velocity crossing a threshold of 0.25 cm/s for at least 1 s,
519 while having been below the threshold for 1 s before. The same criteria were used to define visual flow
520 onsets in the open loop condition using visual flow speed. Visuomotor mismatch responses were probed
521 by presenting brief 1 s full field visual flow halts in the closed loop condition. For a mismatch event to be
522 included in analysis, mice had to be locomoting uninterrupted above threshold (0.25 cm/s) from -0.5 s to
523 +1 s after the event onset. Additionally, for a ROI to be included for analysis of the response to a particular
524 event, it had to have at least 5 onsets to the event.

525 In **Figure 1E**, the calcium responses were baseline subtracted using a -1 s to -0.5 s window relative to
526 locomotion onset and sorted based on the average response in the +0.5 s to +1.5 s activity window. In
527 **Figures 1F-1H,** the activity was averaged over all axons, with a baseline subtraction window of -1 s to -0.5
528 s relative to onset. In **Figure 1I**, the baseline window was -0.5 s to 0 s relative to mismatch onset (to include

529 the locomotion related response in the baseline), and a 95% confidence interval was calculated from
530 randomly drawn timepoints during locomotion. In **Figure 1J**, the locomotion onset response is plotted
531 across different visuomotor conditions, and the baseline window was -1 s to -0.5 s. In **Figure 1K**,
532 cholinergic axons ware classified as responsive to a particular stimulus if the mean activity in a window
533 +0.5 s to +1.5 s after stimulus onset was significantly different (paired two-sample t-test over onsets, $p <$
534 0.05) from the mean of the baseline window (-1 s to -0.5 s).

535 Locomotion offset was defined as the threshold crossing at which locomotion velocity decreased below
536 0.25 cm/s for at least 1 s after mice ran above the threshold for at least 1 s. To isolate locomotion bouts,
537 we identified consecutive locomotion onset and offset events that were separated by at least 4 s. In **Figure**
538 **2C,** we computed correlations in average calcium activity (or locomotion velocity) between locomotion
539 onset and offset across locomotion bouts. Onset responses were defined as the average population
540 activity (or locomotion velocity) +0.5 s to +1.5 s after locomotion onset with a baseline of -1 s to -0.5 s.
541 Offset responses were similarly defined as the average population activity (or locomotion velocity) over -
542 1.5 s to -0.5 s before locomotion offset with the same baseline as for bout onset. In **Figure 2D,** axons were
543 sorted based on their average activity at locomotion onset (defined as above), and the same sort order
544 was preserved for plotting the average activity during the bout and at bout offset. In **Figure 2E**, locomotion
545 velocity was binned into 100 evenly spaced bins in the range of 0 cm/s to 6.25 cm/s, and the activity of
546 cholinergic axons in each bin was averaged. In **Figure 2F**, the correlation of the activity of each cholinergic
547 axon was computed against the mouse locomotion velocity, and this was compared against the
548 correlation computed with a binarized version of locomotion velocity, binarized using a threshold of 0.25
549 cm/s.

550 In **Figures 3B, 3C and S4B** with pupil data, we excluded frames with blinks. For variability and correlation
551 analysis involving pupil diameter, sites with less than 30 s of pupil data in a visuomotor condition were
552 excluded.

553 In **Figures 4A-4H**, to probe for the influence of cholinergic stimulation on responses in visual cortex, the
554 optogenetic stimulation laser was turned on for 1 s coincident with the onset of mismatch or grating
555 stimuli. Further, to isolate the influence of cholinergic stimulation based on the locomotion state, an
556 instance of grating stimulus presentation was defined as occurring during 'locomotion' if mice had a
557 locomotion velocity that was above a threshold (0.25 cm/s) in the time-window of -0.5 s to +1 s from the
558 stimulus onset, otherwise it was defined as occurring while the mouse was 'stationary'. Note, the same
559 criteria to define locomotion state was used to isolate visuomotor mismatches, and also during control

optogenetic stimulation experiments (**Figures S7A-S7E**). For stimulation on locomotion onset, we detected locomotion onsets based on locomotion velocity in real-time. The average delay between locomotion onsets and laser stimulation onsets was 406 ms ± 41 ms (mean ± SEM). For **Figure S6**, we selected the 10% most responsive neurons to gratings, visuomotor mismatch, and locomotion onset. This selection was based on their mean response over half of the trials without optogenetic stimulation (response window: +0.5 s to +2.0 s; baseline window: -0.5 s to 0 s from stimulus onset). We then compared their response over the remaining trials to those with optogenetic stimulation.

In **Figure S8**, for each neuron, we determined the preferred orientation using half the trials while the mice were stationary, and plotted responses relative to this preferred orientation in the other half of the stationary trials, or while the mice were locomoting, or during optogenetic stimulation of cholinergic axons while stationary. As before, a velocity threshold of 0.25 cm/s was used to separate stationary trials from locomoting.

In **Figures 6A-6F**, to compute the average pairwise correlation in activity of neurons, we first split the activity trace based on the locomotion state of the mouse and the presence of optogenetic stimulation. Then, for each condition, we computed the average over all pairwise correlations of a given neuron with every other neuron from the same imaging site. For the chemogenetic experiment, we further compared the change in average pairwise correlation before and after injection of the DREADD ligand. We only included those sites in this analysis which had at least 15 s behavior for each of the two compared conditions.

We defined latency to activation on locomotion onset (**Figure S1**) for a neuron or axon as the time after onset when the calcium activity, averaged across onsets, first was 2 standard deviations above baseline, and remained above this threshold thereafter for at least 1 s. Neurons that did not reach threshold within the analysis window -2 s to +3 s and were not significantly responsive to locomotion onset (paired two-sample t-test over onsets, $p < 0.05$, between baseline -1 s to -0.5 s and response +0.5 s to +1.5 s), were not included in the analysis.

Response latency to grating stimuli (**Figure 7**) was defined for a neuron as the time after onset when the calcium activity, averaged across onsets, first was 2 standard deviations above baseline, and remained above this threshold for at least 1/3 s. Neurons that did not reach threshold within the analysis window of 0 s to +2 s (equal to the duration of grating presentation) were not included in the analysis.

589 **Statistical Analysis.** All statistical information for the tests performed in the manuscript is provided in
590 **Table S1**. Unless stated otherwise, the shading indicates the standard error of the mean across axons or
591 neurons. For analysis where the experimental unit was axon, neuron, or pair of neurons, we used
592 hierarchical bootstrap (Saravanan et al., 2020) for statistical testing due to the nested nature
593 (axons/neurons and mice) of the data. Briefly, we first resampled the data (with replacement) at the level
594 of imaging sites, and then, from the selected sites, resampled for axons (or neurons or neuron pairs). We
595 then computed the mean of this bootstrap sample and repeated this 10 000 times (or 1000 times when
596 comparing response traces in **Figures 4, S6 and S7**) to generate a bootstrap distribution of the mean
597 estimate. For paired tests, the p-value was defined as the proportion of bootstrap samples higher (or
598 lower, depending on the hypothesis) than zero. For unpaired tests, the distribution of the mean for the
599 two variables were compared as the proportion of values higher (or lower, depending on the hypothesis).
600 For analysis where the experimental unit was imaging site, we first tested for normality using Kolmogorov-
601 Smirnov test at a significance level of 5%. For datasets that did not pass the test for normality, the medians
602 were compared with Wilcoxon rank-sum test or signed rank test, as applicable. Otherwise, the means
603 were compared using paired or unpaired t-test, as applicable.

604

605 **Supplemental tables**

606 **Table S1. Statistical information on all analysis.**

607 For statistical comparisons we used paired or unpaired t-tests, or hierarchical bootstraps as indicated in
608 the table below. The units (ROIs, sites, or mice) over which testing was done are boldfaced. For
609 hierarchical bootstraps the two levels of units used are boldfaced.

Figure panel	Value compared	Mean 1	SD 1	Mean 2	SD 2	Test	P-value	N (ROIs)	N (Sites)	N (Mice)
1K	Fraction of responsive cholinergic axons responsive to locomotion onsets *vs* grating onsets	0.523	0.220	0.063	0.075	t-test	$<10^{-5}$	-	**25**	14
	Fraction of responsive cholinergic axons responsive to locomotion onsets *vs* mismatch onsets	0.523	0.220	0.062	0.051	t-test	$<10^{-5}$	-	**25**	14
	Fraction of responsive cholinergic axons responsive to locomotion onsets	0.523	0.220	-	-	t-test	$<10^{-5}$	-	**25**	14
	Fraction of responsive cholinergic axons responsive to grating onsets	0.063	0.075	-	-	t-test	0.40	-	**25**	14
	Fraction of responsive cholinergic axons responsive to mismatch onsets	0.062	0.051	-	-	t-test	0.25	-	**25**	14
2A	Locomotion velocity at locomotion bout onset *vs* offset	0.020	0.008	0.014	0.005	Hierarchical bootstrap	0	**5048**	**25**	14
2B	Cholinergic axon activity [% ΔF/F] at locomotion bout onset *vs* offset	1.47	2.03	1.39	1.80	Hierarchical bootstrap	0.22	**5048**	**25**	14
2C	Correlation between locomotion bout onset and offset for cholinergic axon activity *vs* locomotion velocity	0.554	0.215	0.135	0.258	t-test	$<10^{-5}$	-	**25**	14
2E	Average cholinergic axon activity [% ΔF/F] for low *vs* intermediate locomotion velocity	1.01	0.022	1.01	0.022	Hierarchical bootstrap	0.58	**5048, 3657**	**25, 17**	14, 11
	Average cholinergic axon activity [% ΔF/F] for intermediate *vs* high locomotion velocity	1.01	0.022	1.01	0.008	Hierarchical bootstrap	0.59	**3657, 1282**	**17, 7**	11, 5
	Average cholinergic axon activity [% ΔF/F] for low *vs* high locomotion velocity	1.01	0.022	1.01	0.008	Hierarchical bootstrap	0.70	**5048, 1282**	**25, 7**	14, 5
2F	Correlation of activity of cholinergic axons with raw *vs* binarized velocity	0.083	0.082	0.099	0.092	Hierarchical bootstrap	0	**5048**	**25**	14
3A	Correlation of average cholinergic axon activity with locomotion velocity in closed loop *vs* open loop	0.286	0.170	0.322	0.199	t-test	0.15	-	**25**	14
	Correlation of average cholinergic axon activity with locomotion velocity in dark *vs* grating	0.319	0.200	0.311	0.167	t-test	0.77	-	**25**	14
	Correlation of average cholinergic axon activity with locomotion velocity in closed loop *vs* dark	0.286	0.170	0.319	0.200	t-test	0.27	-	**25**	14
	Correlation of average cholinergic axon activity with locomotion velocity in open loop *vs* grating	0.322	0.199	0.311	0.167	t-test	0.75	-	**25**	14

	Correlation of average cholinergic axon activity with locomotion velocity in open loop *vs* dark	0.322	0.199	0.319	0.200	t-test	0.93	-	**25**	14
	Correlation of average cholinergic axon activity with locomotion velocity in closed loop *vs* grating	0.286	0.170	0.311	0.167	t-test	0.33	-	**25**	14
3B	Correlation of average cholinergic axon activity with pupil diameter in closed loop *vs* open loop	0.165	0.150	0.277	0.170	t-test	0.0001	-	**25**	14
	Correlation of average cholinergic axon activity with pupil diameter in dark *vs* grating	0.002	0.141	0.300	0.136	Unpaired t-test	0.0000	-	**21, 25**	13, 14
	Correlation of average cholinergic axon activity with pupil diameter in closed loop *vs* dark	0.165	0.150	0.002	0.141	Unpaired t-test	0.0005	-	**25, 21**	14, 13
	Correlation of average cholinergic axon activity with pupil diameter in open loop *vs* grating	0.277	0.170	0.300	0.136	t-test	0.61	-	**25**	14
	Correlation of average cholinergic axon activity with pupil diameter in open loop *vs* dark	0.277	0.170	0.002	0.141	Unpaired t-test	0.0000	-	**25, 21**	14, 13
	Correlation of average cholinergic axon activity with pupil diameter in closed loop *vs* grating	0.165	0.150	0.300	0.136	t-test	0.0028	-	**25**	14
3C	Correlation of pupil diameter with locomotion velocity in closed loop *vs* open loop	0.324	0.217	0.457	0.215	t-test	0.0001	-	**25**	14
	Correlation of pupil diameter with locomotion velocity in dark *vs* grating	0.060	0.232	0.435	0.239	Unpaired t-test	0.0000	-	**21, 25**	13, 14
	Correlation of pupil diameter with locomotion velocity in closed loop *vs* dark	0.324	0.217	0.060	0.232	Unpaired t-test	0.0003	-	**25, 21**	14, 13
	Correlation of pupil diameter with locomotion velocity in open loop *vs* grating	0.457	0.215	0.435	0.239	t-test	0.70	-	**25**	14
	Correlation of pupil diameter with locomotion velocity in open loop *vs* dark	0.457	0.215	0.060	0.232	Unpaired t-test	0.0000	-	**25, 21**	14, 13
	Correlation of pupil diameter with locomotion velocity in closed loop *vs* grating	0.324	0.217	0.435	0.239	t-test	0.045	-	**25**	14
4A	Grating response difference in layer 2/3 neurons [% ΔF/F] while locomoting *vs* not locomoting	-0.12	10.66	-1.97	6.78	Hierarchical bootstrap	0	**6529**	**21**	14
4B	Grating response difference in layer 5 neurons [% ΔF/F] while locomoting *vs* not locomoting	3.13	8.10	0.88	5.50	Hierarchical bootstrap	0	**6798**	**25**	14
4C	Grating response difference in layer 2/3 neurons [% ΔF/F] on optogenetic stimulation *vs* no stimulation while not locomoting	-2.43	8.10	-2.44	7.44	Hierarchical bootstrap	0.46	**3992**	**13**	13
4D	Grating response difference in layer 5 neurons [% ΔF/F] on optogenetic stimulation *vs* no stimulation while not locomoting	1.21	6.05	0.62	6.06	Hierarchical bootstrap	0.0060	**4715**	**16**	13
4E	Mismatch response difference in layer 2/3 neurons [% ΔF/F] on optogenetic stimulation vs no stimulation	2.00	10.14	2.25	8.36	Hierarchical bootstrap	0.66	**2506**	**9**	9
4F	Mismatch response difference in layer 5 neurons [% ΔF/F] on optogenetic stimulation *vs* no stimulation	2.72	7.26	1.77	5.30	Hierarchical bootstrap	0.028	**2801**	**9**	6

4G	Locomotion onset response difference in closed loop in layer 2/3 neurons [% ΔF/F] on optogenetic stimulation *vs* no stimulation	1.66	9.36	1.23	5.76	Hierarchical bootstrap	0.13	**2747**	**10**	10
4H	Locomotion onset response difference in closed loop in layer 5 neurons [% ΔF/F] on optogenetic stimulation *vs* no stimulation	2.63	5.54	1.86	4.26	Hierarchical bootstrap	0	**3623**	**11**	8
5A	Mean response in layer 2/3 neurons [% ΔF/F] on locomotion onset *vs* zero	1.82	7.37	-	-	Hierarchical bootstrap	0	**6154**	**20**	14
5B	Mean response in layer 5 neurons [% ΔF/F] on locomotion onset *vs* zero	2.00	4.28	-	-	Hierarchical bootstrap	0	**6032**	**22**	12
5C	Mean response in layer 2/3 neurons [% ΔF/F] to optogenetic stimulation of ChAT axons *vs* zero	-0.07	6.63	-	-	Hierarchical bootstrap	0.62	**6154**	**20**	14
5D	Mean response in layer 5 neurons [% ΔF/F] on optogenetic stimulation of ChAT axons *vs* zero	-0.16	3.21	-	-	Hierarchical bootstrap	0.86	**6032**	**22**	13
6E	Difference in average pairwise correlation of layer 2/3 neurons while locomoting *vs* not locomoting	0.035	0.020	0.038	0.021	Hierarchical bootstrap	0.045	**7826**	**25**	15
	Difference in average pairwise correlation of layer 2/3 neurons on optogenetic stimulation *vs* no stimulation while not locomoting	0.021	0.018	0.029	0.022	Hierarchical bootstrap	0	**1688**	**4**	4
6F	Difference in average pairwise correlation of layer 5 neurons while locomoting *vs* not locomoting	0.030	0.017	0.036	0.017	Hierarchical bootstrap	$<10^{-3}$	**7132**	**26**	14
	Difference in average pairwise correlation of layer 5 neurons on optogenetic stimulation *vs* no stimulation while not locomoting	0.009	0.010	0.014	0.009	Hierarchical bootstrap	0.0017	**100**	**4**	4
6G	Layer 2/3 neuron difference in the change in average pairwise correlation on locomotion following ligand injection for DREADD activation *vs* inhibition	-0.0005	$<10^{-3}$	-0.002	$<10^{-3}$	Hierarchical bootstrap	0.32	**2429, 3103**	**7, 10**	7, 9
6H	Layer 5 neuron difference in the change in average pairwise correlation on locomotion following ligand injection for DREADD activation *vs* inhibition	-0.003	$<10^{-3}$	0.007	$<10^{-3}$	Hierarchical bootstrap	0.032	**1651, 1762**	**7, 7**	7, 7
7A	Latency to grating response onset in layer 2/3 neurons [ms] while locomoting *vs* not locomoting	596	470	632	451	Hierarchical bootstrap	0.86	**1481**	**24**	15
	Latency to grating response onset in layer 2/3 neurons [ms] on optogenetic stimulation *vs* no stimulation while not locomoting	656	427	659	444	Hierarchical bootstrap	0.54	**1503**	**15**	15
7B	Latency to grating response onset in layer 5 neurons [ms] while locomoting *vs* not locomoting	658	413	771	417	Hierarchical bootstrap	0.0037	**938**	**25**	14
	Latency to grating response onset in layer 5 neurons [ms] on optogenetic stimulation *vs* no stimulation while not locomoting	709	407	793	413	Hierarchical bootstrap	0.0046	**783**	**16**	13
S1D	Latency to response on locomotion onset [ms] for cholinergic axons *vs* layer 2/3 neurons	477	457	366	614	Hierarchical bootstrap	0.040	**1182, 1166**	**23, 25**	12, 15
	Latency to response on locomotion onset [ms] for cholinergic axons *vs* layer 5 neurons	477	457	635	503	Hierarchical bootstrap	0.014	**1182, 1299**	**23, 26**	12, 14

	Latency to response on locomotion onset [ms] for layer 2/3 neurons *vs* layer 5 neurons	366	614	635	503	Hierarchical bootstrap	0	**1166, 1299**	**25, 26**	15, 14
S2G	Correlation of cholinergic axon population activity vector between bout onset and during the bout for actual *vs* random triggers	0.735	0.187	0.007	0.088	t-test	$<10^{-5}$	-	**25**	14
	Correlation of cholinergic axon population activity vector between during the bout and at bout onset for actual *vs* random triggers	0.759	0.194	0.036	0.120	t-test	$<10^{-5}$	-	**25**	14
	Correlation of cholinergic axon population activity vector between bout onset and offset for actual *vs* random triggers	0.721	0.196	0.012	0.103	t-test	$<10^{-5}$	-	**25**	14
S2H	Average GRAB-ACh activity [% ΔF/F] in visual cortex during low *vs* high velocity	1.3	3.4	0.22	3.9	Hierarchical bootstrap	0.7	**178, 132**	**8,6**	8,6
S4A	Variability in pupil diameter [SD] in closed loop *vs* open loop	21.32	8.47	18.68	5.48	t-test	0.15	-	**25**	14
	Variability in pupil diameter [SD] in dark *vs* grating	25.52	17.45	16.54	7.16	Unpaired t-test	0.023	-	**21, 25**	13, 14
	Variability in pupil diameter [SD] in closed loop *vs* dark	21.32	8.47	25.52	17.45	Unpaired t-test	0.29	-	**25, 21**	14, 13
	Variability in pupil diameter [SD] in open loop *vs* grating	18.68	5.48	16.54	7.16	t-test	0.10	-	**25**	14
	Variability in pupil diameter [SD] in open loop *vs* dark	18.68	5.48	25.52	17.45	Unpaired t-test	0.070	-	**25, 21**	14, 13
	Variability in pupil diameter [SD] in closed loop *vs* grating	21.32	8.47	16.54	7.16	t-test	0.041	-	**25**	14
S4B	Correlation of average cholinergic axon activity with locomotion velocity *vs* facial movement in closed loop	0.286	0.170	0.095	0.172	t-test	$<10^{-4}$	-	**25**	14
	Correlation of average cholinergic axon activity with locomotion velocity *vs* facial movement in open loop	0.322	0.199	0.148	0.195	t-test	0.0001	-	**25**	14
	Correlation of average cholinergic axon activity with locomotion velocity *vs* facial movement in dark	0.319	0.200	0.090	0.224	t-test	$<10^{-4}$	-	**25**	14
	Correlation of average cholinergic axon activity with locomotion velocity *vs* facial movement in grating condition	0.311	0.167	0.130	0.214	t-test	0.0001	-	**25**	14
S5A	Mice locomotion velocity [cm/s] on optogenetic stimulation of cholinergic axons, before *vs* after	2.53	3.09	2.4	3.09	Hierarchical bootstrap	0.81	-	**51, 51**	15, 15
S5B	Average locomotion velocity [cm/s], before *vs* upon optogenetic stimulation of cholinergic axons in visual cortex	2.53	3.09	2.4	3.09	Hierarchical bootstrap	0.81	-	**51, 51**	15, 15
S6A	Grating response difference in 10% highest grating responsive layer 2/3 neurons [% ΔF/F] on optogenetic stimulation *vs* no stimulation while not locomoting	4.87	12.36	5.47	11.87	Hierarchical bootstrap	0.74	**399**	**13**	13
S6B	Mismatch response difference in layer 2/3 neurons [% ΔF/F] on optogenetic stimulation vs no stimulation	8.47	19.46	9.57	25.84	Hierarchical bootstrap	0.68	**251**	**9**	9
S6C	Locomotion onset response difference in closed loop in layer 2/3 neurons [% ΔF/F] on	11.05	16.99	9.94	10.56	Hierarchical bootstrap	0.23	**275**	**10**	10

	optogenetic stimulation *vs* no stimulation									
S7F	Change in average pairwise correlation of layer 2/3 neuron on control stimulation *vs* no stimulation while not locomoting	0.025	0.030	0.025	0.022	Hierarchical bootstrap	0.46	**1047**	**3**	3
	Change in average pairwise correlation of layer 5 neurons on control stimulation *vs* no stimulation while not locomoting	0.017	0.021	0.012	0.006	Hierarchical bootstrap	0.18	**88**	**3**	3
S8A	Mean response in layer 2/3 neurons [% ΔF/F] to grating onset (preferred + π/4 Ori) stationary *vs* locomotion	-3.10	9.36	-0.30	9.95	Hierarchical bootstrap	0	**2396, 2500**	**13, 13**	13, 13
	Mean response in layer 2/3 neurons [% ΔF/F] to grating onset (preferred Ori) stationary *vs* locomotion	-1.50	12.87	1.80	18.57	Hierarchical bootstrap	0	**3908, 3992**	**13, 13**	13, 13
	Mean response in layer 2/3 neurons [% ΔF/F] to grating onset (preferred - π/4 Ori) stationary *vs* locomotion	-2.67	9.84	-0.84	11.83	Hierarchical bootstrap	0.002	**2729, 2729**	**13, 13**	13, 13
	Mean response in layer 2/3 neurons [% ΔF/F] to grating onset (preferred + π/2 Ori) stationary *vs* locomotion	-2.64	9.04	-0.92	13.97	Hierarchical bootstrap	0.009	**2519, 2572**	**13, 13**	13, 13
	Mean response in layer 2/3 neurons [% ΔF/F] to grating onset (preferred + π/4 Ori) stationary *vs* (stationary + opto)	-3.10	9.36	-2.50	6.95	Hierarchical bootstrap	0.08	**2396, 2500**	**13, 13**	13, 13
	Mean response in layer 2/3 neurons [% ΔF/F] to grating onset (preferred Ori) stationary *vs* (stationary + opto)	-1.50	12.87	-1.33	10.54	Hierarchical bootstrap	0.27	**3908, 3992**	**13, 13**	13, 13
	Mean response in layer 2/3 neurons [% ΔF/F] to grating onset (preferred - π/4 Ori) stationary *vs* (stationary + opto)	-2.67	9.84	-2.59	7.61	Hierarchical bootstrap	0.42	**2729, 2729**	**13, 13**	13, 13
	Mean response in layer 2/3 neurons [% ΔF/F] to grating onset (preferred + π/2 Ori) stationary *vs* (stationary + opto)	-2.64	9.04	-2.22	8.33	Hierarchical bootstrap	0.32	**2519, 2572**	**13, 13**	13, 13
S8B	Mean response in layer 5 neurons [% ΔF/F] to grating onset (preferred + π/4 Ori) stationary *vs* locomotion	-0.26	10.40	2.01	10.72	Hierarchical bootstrap	10^{-4}	**3448, 3520**	**16, 16**	13, 13
	Mean response in layer 5 neurons [% ΔF/F] to grating onset (preferred Ori) stationary *vs* locomotion	0.28	11.76	4.49	15.16	Hierarchical bootstrap	0	**4670, 4715**	**16, 16**	13, 13
	Mean response in layer 5 neurons [% ΔF/F] to grating onset (preferred - π/4 Ori) stationary *vs* locomotion	-0.28	9.58	2.77	9.74	Hierarchical bootstrap	0	**3518, 3614**	**16, 16**	13, 13
	Mean response in layer 5 neurons [% ΔF/F] to grating onset (preferred + π/2 Ori) stationary *vs* locomotion	-0.83	8.85	2.33	9.66	Hierarchical bootstrap	0	**3642, 3642**	**16, 16**	13, 13
	Mean response in layer 5 neurons [% ΔF/F] to grating onset (preferred + π/4 Ori) stationary *vs* (stationary + opto)	-0.26	10.40	-0.10	7.18	Hierarchical bootstrap	0.30	**3448, 3520**	**16, 16**	13,
	Mean response in layer 5 neurons [% ΔF/F] to grating onset (preferred Ori) stationary *vs* (stationary + opto)	0.28	11.76	1.37	9.62	Hierarchical bootstrap	0	**4670, 4715**	**16, 16**	13, 13
	Mean response in layer 5 neurons [% ΔF/F] to grating onset (preferred	-0.28	9.58	0.14	7.23	Hierarchical bootstrap	0.13	**3518, 3614**	**16, 16**	13, 13

	- π/4 Ori) stationary *vs* (stationary + opto)									
	Mean response in layer 5 neurons [% ΔF/F] to grating onset (preferred + π/2 Ori) stationary *vs* (stationary + opto)	-0.83	8.85	-0.53	6.02	Hierarchical bootstrap	0.22	**3642, 3642**	**16, 16**	13, 13
S11 B	Locomotion velocity before *vs* after DREADD activation	0.022	0.005	0.028	0.005	t-test	$<10^{-3}$	-	**14**	7
	Locomotion velocity before *vs* after DREADD inhibition	0.017	0.004	0.016	0.005	t-test	0.46	-	**17**	9
S11 D	Time spent locomoting before *vs* after DREADD activation	0.683	0.143	0.699	0.154	t-test	0.64	-	**14**	7
	Time spent locomoting before *vs* after DREADD inhibition	0.572	0.156	0.360	0.164	t-test	$<10^{-5}$	-	**17**	9
S11E	Total distance run before *vs* after DREADD activation	5.086	1.964	6.511	2.457	t-test	0.0067	-	**14**	7
	Total distance run before *vs* after DREADD inhibition	3.314	1.713	2.144	1.413	t-test	$<10^{-4}$	-	**17**	9
	Change in total distance run on DREADD activation *vs* inhibition	1.425	1.657	-1.170	0.913	Unpaired t-test	$<10^{-5}$	-	**14, 17**	7, 9
S12 A	Change in average pairwise correlation on locomotion in layer 2/3 neurons in DREADD activation group pre-CNO *vs* zero	-0.010	0.019	-	-	Hierarchical bootstrap	0	**2429**	**7**	**7**
	Change in average pairwise correlation on locomotion in layer 2/3 neurons in DREADD activation group post-CNO *vs* zero	-0.010	0.019	-	-	Hierarchical bootstrap	10^{-4}	**2429**	**7**	**7**
	Change in average pairwise correlation on locomotion in layer 2/3 neurons in DREADD inhibition group pre-CNO *vs* zero	-0.004	0.019	-	-	Hierarchical bootstrap	0.01	**3103**	**10**	9
	Change in average pairwise correlation on locomotion in layer 2/3 neurons in DREADD inhibition group post-CNO *vs* zero	-0.006	0.020	-	-	Hierarchical bootstrap	0.02	**3103**	**10**	9
S12 B	Change in average pairwise correlation on locomotion in layer 5 neurons in DREADD activation group pre-CNO *vs* zero	-0.008	0.016	-	-	Hierarchical bootstrap	0	**1651**	**7**	**7**
	Change in average pairwise correlation on locomotion in layer 5 neurons in DREADD activation group post-CNO *vs* zero	-0.011	0.019	-	-	Hierarchical bootstrap	0.003	**1651**	**7**	**7**
	Change in average pairwise correlation on locomotion in layer 5 neurons in DREADD inhibition group pre-CNO *vs* zero	-0.010	0.020	-	-	Hierarchical bootstrap	0.001	**1762**	**7**	**7**
	Change in average pairwise correlation on locomotion in layer 5 neurons in DREADD inhibition group post-CNO *vs* zero	-0.002	0.016	-	-	Hierarchical bootstrap	0.23	**1762**	**7**	**7**

611 **Table S2. Number of mice in different experimental groups**

Genotype	Virus	Site of injection	Nbr. Mice	Nbr. ROIs	Figures
ChAT-IRES-Cre	AAV2/5-hSyn1-FLEx-axon-GCaMP6s	Basal forebrain – MS/vDB/hDB	12	4451	Figures 1, 2, 3, S1, S2G, S3, S4
ChAT-IRES-Cre	AAV PHP.eB-Ef1α-DIO-GCaMP6s	Basal forebrain – MS/vDB/hDB	2	597	Figures 1, 2, 3, S1, S2G, S3, S4
ChAT-IRES-Cre	AAV2/1-hSyn-DIO-ChrimsonR-tdTomato	Basal forebrain – MS/vDB/hDB	15	15 103	Figures 4, 5, 6A-6F, 7, S1, S5, S6, S7D-S7F, S8, S9, S10, S13
	AAV2/1-Ef1α-GCaMP6f-WPRE	Primary visual cortex			
ChAT-IRES-Cre	AAV2/1-Ef1α-DIO-hM3D(Gq)-mCherry	Basal forebrain – MS/vDB/hDB	7	4080	Figures 6G-6H, S11, S12
	AAV2/1-Ef1α-GCaMP6f-WPRE	Primary visual cortex			
ChAT-IRES-Cre	AAV2/1-Ef1α-DIO-hM4D(Gi)-mCherry	Basal forebrain – MS/vDB/hDB	9	4865	Figures 6G-6H, S11, S12
	AAV2/1-Ef1α-GCaMP6f-WPRE	Primary visual cortex			
ChAT-IRES-Cre	AAV2/9-hSyn-GRAB-ACh3.0	Primary visual cortex	8	609	Figures S2A-S2C, S2H
ChAT-IRES-Cre	AAV2/1-Ef1α-DIO-tdTomato-WPRE	Basal forebrain – MS/vDB/hDB	5	2409	Figures S7A-S7C
	AAV2/1-Ef1α-GCaMP6f-WPRE	Primary visual cortex			
ChAT-IRES-Cre	AAV2/1-Ef1α-eGFP-WPRE	Primary visual cortex	6	2640	Figures S2D-S2F

612

FIGURES

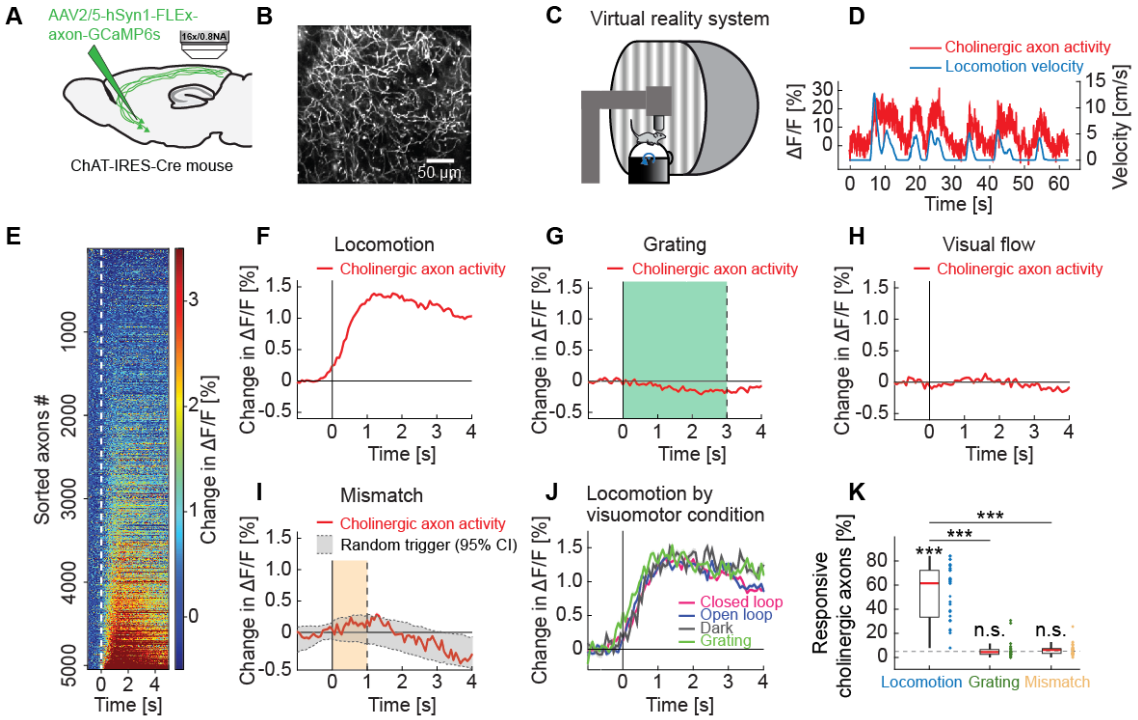

Figure 1. Cholinergic axons in visual cortex are activated during locomotion independent of visual stimuli.

(**A**) GCaMP6s was expressed by injecting an AAV2/5-hSyn1-FLEx-axon-GCaMP6s vector in basal forebrain of ChAT-IRES-Cre mice. We then imaged calcium activity of cholinergic axons projecting to visual cortex.

(**B**) Example two-photon image of cholinergic axons in visual cortex.

(**C**) Schematic of the virtual reality system. Mice were head-fixed on a spherical treadmill and surrounded by a toroidal screen on which we presented visual stimuli in different visuomotor conditions.

(**D**) Example trace of the calcium activity of one cholinergic axon in visual cortex (red) and the corresponding locomotion velocity of the mouse (blue).

(**E**) Average locomotion onset activity of all cholinergic axons (5048 axons in 14 mice), sorted by their average response during locomotion onset.

(**F**) Average response of cholinergic axons to locomotion onset over all the cholinergic axons, of the data shown in **E**. Shading indicates SEM over axons. Due to SEM being very small, the shading is fully obscured by the red line.

(**G**) As in **F**, but for grating onsets. Green shading marks the duration of grating presentation.

(**H**) As in **F**, but for visual flow onset during the open loop condition.

(**I**) As in **F**, but for visuomotor mismatch onset. Orange shading marks the duration of visuomotor mismatch. As mismatch events occur only during times of locomotion, and locomotion itself is a strong driver of cholinergic activity, we would expect to find an increase in cholinergic activity by chance at

634 mismatch. To correct for this, we quantified the distribution of cholinergic activity on random triggers
635 during locomotion (95% confidence interval (CI), gray shading).

636 (**J**) Locomotion onset activity in different visuomotor conditions.
637
638 (**K**) The fraction of cholinergic axons responsive to locomotion, grating, and visuomotor mismatch onset,
639 quantified for each imaging site. Each datapoint is one imaging site. Boxes show 25th and 75th percentile,
640 central mark is the median, and the whiskers extend to the most extreme datapoints not considered
641 outliers. Dashed line marks chance level. n.s.: not significant; *: $p < 0.05$; **: $p < 0.01$; ***: $p < 0.001$; see
642 **Table S1** for all statistical information.

643

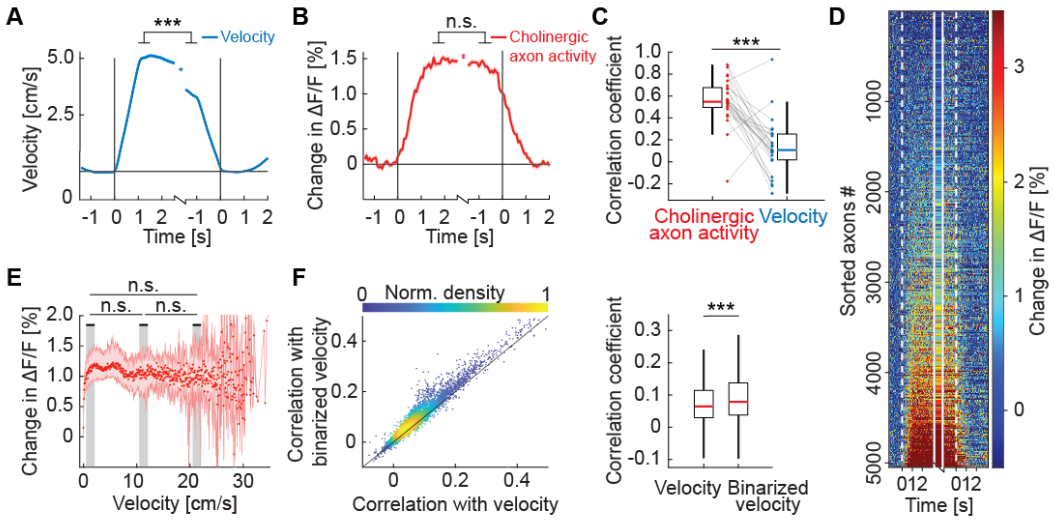

Figure 2. Activity in cholinergic axons was better explained by a binary locomotion state signal than by locomotion velocity.

(**A**) Average locomotion velocity profiles aligned to locomotion onset and offset. The isolated datapoint between the two traces is the average locomotion velocity over the locomotion bout. Shading marks SEM. Here and elsewhere, n.s.: not significant; *: p<0.05; **: p<0.01; ***: p<0.001; see **Table S1** for all statistical information.

(**B**) As in **A**, but for activity of all cholinergic axons in visual cortex, for the data shown in **D**. Shading marks SEM over axons.

(**C**) Bout-by-bout correlation coefficient between the locomotion onset and offset changes for average cholinergic activity and locomotion velocity. Each datapoint is one imaging site. Boxes show 25th and 75th percentile, central mark is the median, and the whiskers extend to the most extreme datapoints not considered outliers.

(**D**) Average onset and offset responses for all cholinergic axons sorted by strength of locomotion onset response.

(**E**) Activity of cholinergic axons as a function of locomotion velocity. Shown are the hierarchical bootstrap estimates of the median (red dots) and 95% confidence intervals (red shading) for each velocity bin. We found no evidence of a difference in activation between low, intermediate, and high locomotion velocities (indicated by gray shading).

(**F**) Left: For all axons, the correlation coefficient of their calcium activity with locomotion velocity plotted against the correlation coefficient with a binarized version of the locomotion velocity. Right: Distributions of correlation coefficients between calcium activity and locomotion velocity and binarized velocity. Same data as shown on the left. Boxes show 25th and 75th percentile, central mark is the median, and the whiskers extend to the most extreme datapoints not considered outliers.

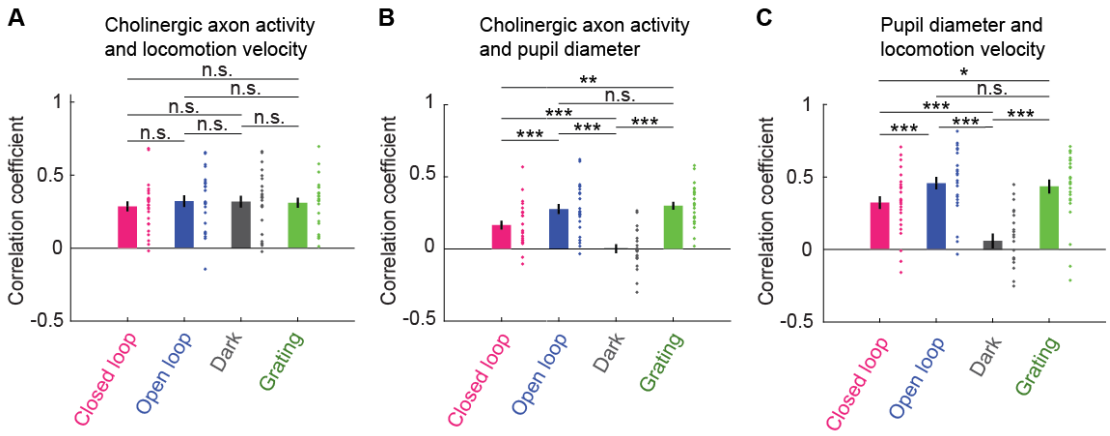

669

670 **Figure 3. Average activity of cholinergic axons was more strongly correlated with locomotion velocity**
671 **than with pupil diameter.**

672 (**A**) Correlation of average activity of cholinergic axons activity with locomotion velocity in closed loop,
673 open loop, dark, and grating conditions. Each point represents data from one imaging site, error bars
674 indicate SEM. Here and elsewhere, n.s.: not significant; *: $p < 0.05$; **: $p < 0.01$; ***: $p < 0.001$; see **Table**
675 **S1** for all statistical information.

676 (**B**) As in **A**, but for correlation between average activity of cholinergic axons and pupil diameter.

677 (**C**) As in **A**, but for correlation between locomotion velocity and pupil diameter.

678

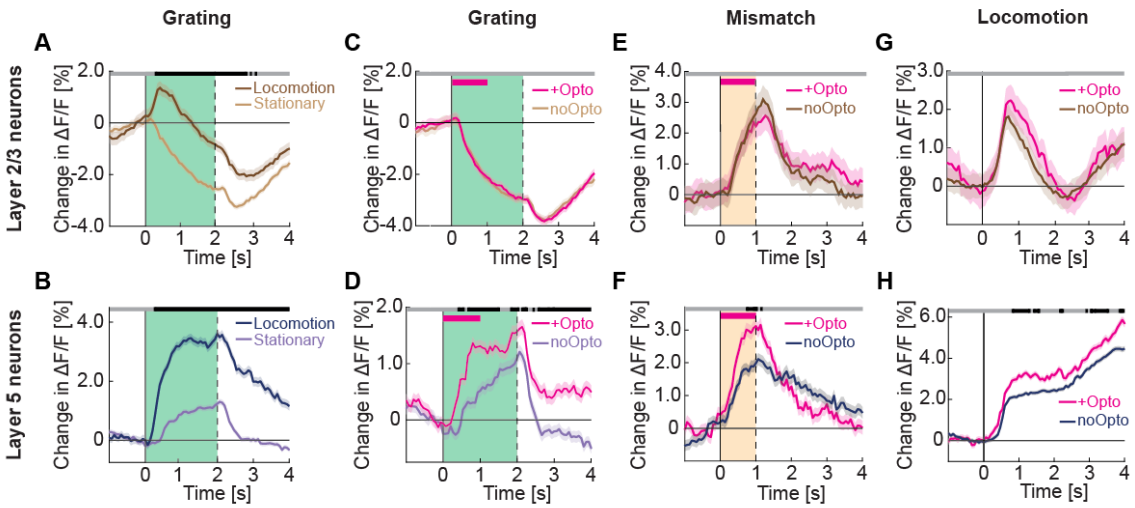

679

680 **Figure 4. Optogenetic activation of cholinergic axons in visual cortex primarily enhances responses of**
681 **layer 5, but not layer 2/3 neurons.**

682 (**A**) Average calcium response of layer 2/3 neurons in visual cortex to full field drifting gratings in the
683 absence (light brown) or presence of locomotion (brown). Green shading indicates duration of grating
684 stimulus. The responses are compared bin-by-bin using a nested hierarchical bootstrap test. Here and in
685 subsequent panels, bins with a significant difference ($p < 0.05$) are indicated by a black line above the plot;
686 those with $p > 0.05$ are marked gray. Shading marks SEM.

687 (**B**) As in **A**, but for layer 5 neurons in visual cortex in the absence (light blue) or presence (dark blue) of
688 locomotion.

689 (**C**) Average calcium response of layer 2/3 neurons in visual cortex to full field drifting gratings while the
690 mice were stationary, without (light brown) or with (pink) optogenetic activation of cholinergic axons in
691 visual cortex. Duration of optogenetic stimulation is marked by a pink bar. Green shading indicates
692 duration of the grating stimulus.

693 (**D**) As in **C**, but for layer 5 neurons in visual cortex.

694 (**E**) Average calcium response to visuomotor mismatch in layer 2/3 neurons in visual cortex, without
695 (brown) and with (pink) optogenetic stimulation of cholinergic axons in visual cortex. Orange shading
696 indicates mismatch duration, and pink bar indicates optogenetic stimulation.

697 (**F**) As in **E**, but for layer 5 neurons in visual cortex.

698 (**G**) Average calcium response of layer 2/3 neurons in visual cortex to locomotion onset in closed loop,
699 without (brown) or with (pink) optogenetic stimulation of cholinergic axons in visual cortex.

700 (**H**) As in **G**, but for layer 5 neurons in visual cortex.

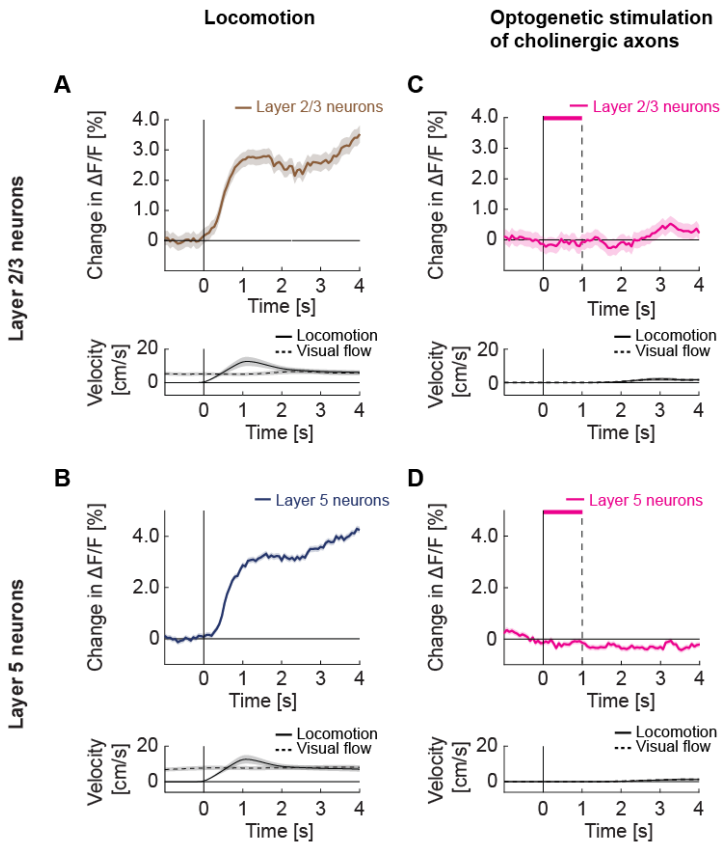

Figure 5. Optogenetic activation of cholinergic axons in visual cortex did not drive responses in either layer 2/3 or layer 5 neurons.

(**A**) Upper panel: Average calcium response of layer 2/3 neurons in visual cortex to locomotion onset in open loop. Lower panel: Average locomotion velocity and visual flow speed for the corresponding onsets. Shading indicates SEM.

(**B**) As in **A**, but for layer 5 neurons in visual cortex.

(**C**) Upper panel: Average calcium response of layer 2/3 neurons in visual cortex during local optogenetic stimulation of cholinergic axons while the mice were stationary. Pink bar marks duration of the optogenetic stimulus. Lower panel: Average locomotion velocity and visual flow speed for the corresponding onsets. Note, the two overlap by experimental design.

(**D**) As in **C**, but for layer 5 neurons in visual cortex.

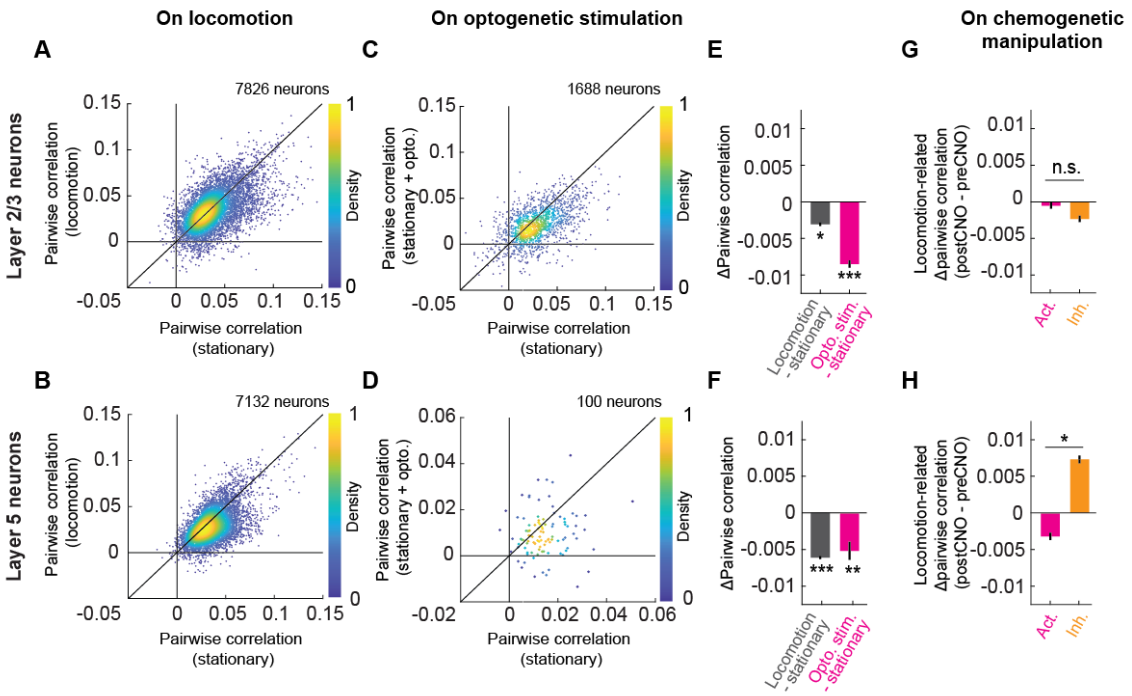

Figure 6. Cholinergic axon activation reduced pairwise correlations between neurons in visual cortex.

(**A**) Average pairwise correlation in calcium activity of layer 2/3 neurons while the mouse was stationary and while the mouse was locomoting. Each dot is the mean of the pairwise correlations for one neuron to all others in the same field of view.

(**B**) As in **A**, but for layer 5 neurons.

(**C**) As in **A**, but comparing the correlation while the mice were stationary, to that while cholinergic axons were stimulated optogenetically.

(**D**) As in **C**, but for layer 5 neurons. Note, for this experiment the imaging plane was in L2/3 to simultaneously image layer 2/3 neurons and apical dendrites of layer 5. The latter were traced to their soma in layer 5 offline and were used to compute layer 5 activity correlations.

(**E**) Average change in pairwise correlations of layer 2/3 neurons on locomotion (gray) or on optogenetic stimulation of cholinergic axons during stationary periods (pink), compared to the correlations during stationary (stat.) periods at baseline. Here and elsewhere, n.s.: not significant; *: $p < 0.05$; **: $p < 0.01$; ***: $p < 0.001$; see **Table S1** for all statistical information.

(**F**) As in **E**, but for layer 5 neurons of visual cortex.

(**G**) Change in the average pairwise correlations of layer 2/3 neurons during locomotion, upon DREADD activation (pink) or inhibition (orange) of basal forebrain cholinergic neurons.

(**H**) As in **G**, but for layer 5 neurons.

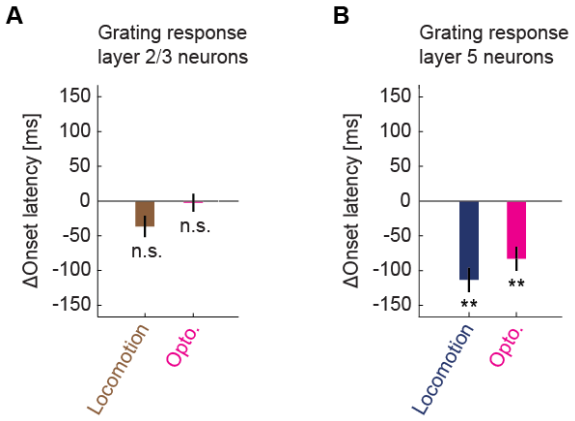

Figure 7. Cholinergic input reduced response latency of layer 5 neurons in visual cortex to grating stimuli.

(**A**) Locomotion (brown) or optogenetic stimulation of cholinergic axons (pink) induced change in the response latency of layer 2/3 neurons in visual cortex to full field drifting grating onset. Here and elsewhere, n.s.: not significant; *: $p<0.05$; **: $p<0.01$; ***: $p<0.001$; see **Table S1** for all statistical information.

(**B**) As in **A**, but for layer 5 neurons.

743 **SUPPLEMENTARY FIGURES**

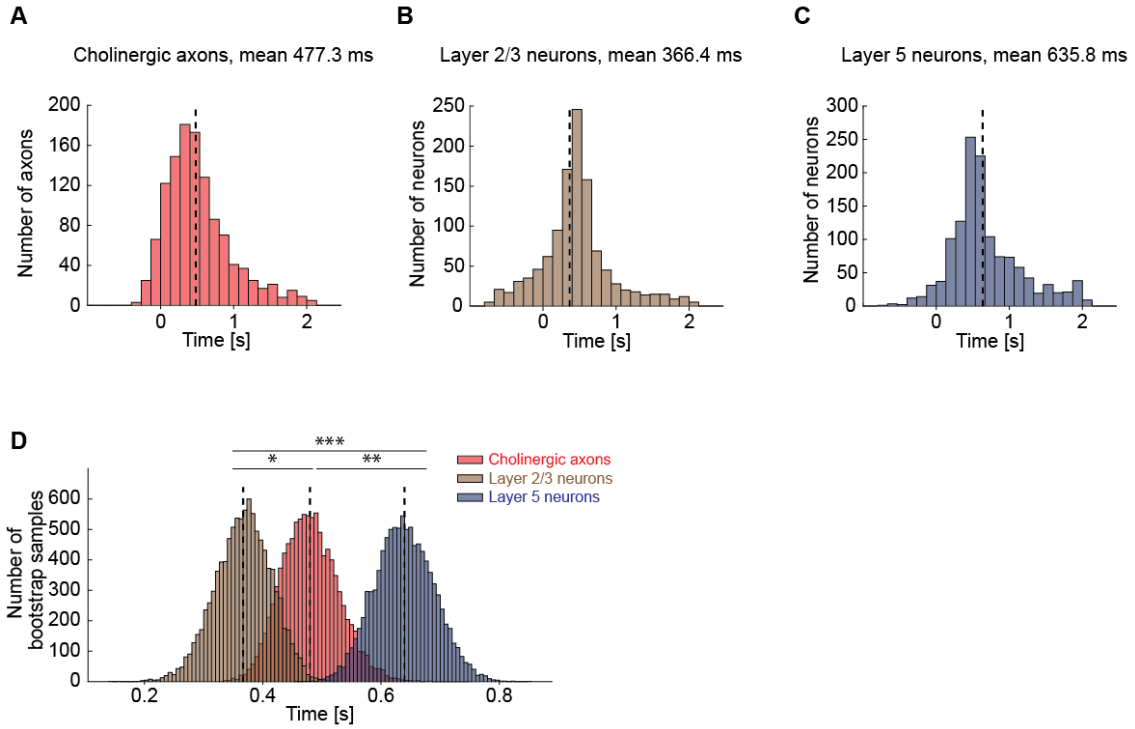

744

745 **Figure S1. Cholinergic axons in visual cortex were activated after layer 2/3 but before layer 5 visual**
746 **cortex neurons. Related to Figure 1.**

747 (**A**) Distribution of time to first significant response after locomotion onset for cholinergic axons in visual
748 cortex. Axons without any response to locomotion onset are omitted.

749 (**B**) As in **A**, but for layer 2/3 neurons in visual cortex.

750 (**C**) As in **A**, but for layer 5 neurons in visual cortex.

751 (**D**) Nested bootstrap resampling of the distributions shown in **A-C**. Here and elsewhere, n.s.: not
752 significant; *: p<0.05; **: p<0.01; ***: p<0.001; see **Table S1** for all statistical information.

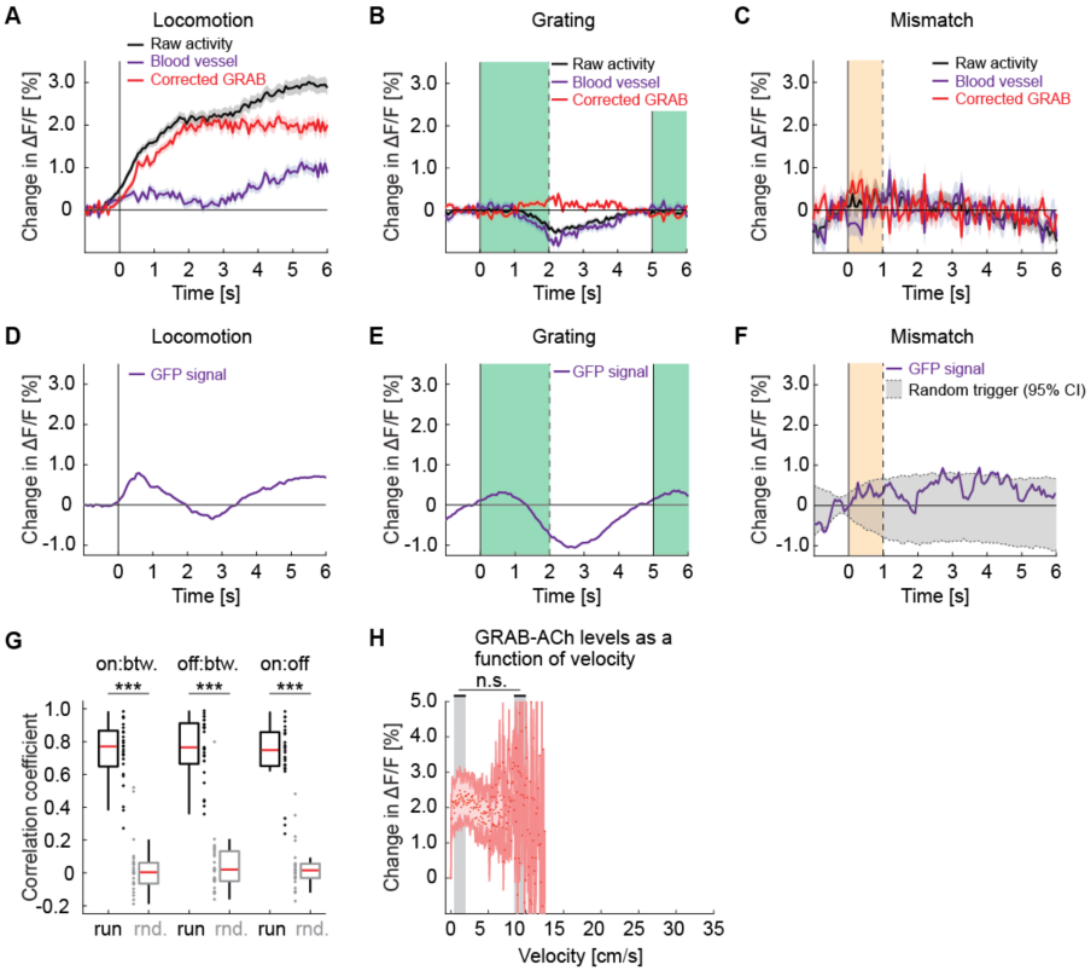

Figure S2. Responses of GRAB-ACh3.0 in visual cortex are similar to the calcium responses in cholinergic axons. Related to Figure 2.

(**A**) Average change in GRAB-ACh3.0 fluorescence during locomotion onset. We used the fluorescence change measured in blood vessels (purple) to estimate hemodynamic occlusion and subtracted this from the raw activity (black) to generate a corrected response (red). Shading marks SEM.

(**B**) As in **A**, but for the GRAB-ACh3.0 response to grating onsets. The green shading marks the duration of the grating stimulus.

(**C**) As in **A**, but for the GRAB-ACh3.0 response to visuomotor mismatch. The orange shading marks the duration of the visuomotor mismatch.

(**D**) To estimate hemodynamic occlusion effects while two-photon imaging, we measured fluorescence changes on locomotion onset in layer 2/3 neurons in visual cortex that express GFP.

(**E**) As in **D**, but for responses to grating onsets.

(**F**) As in **D**, but for responses to visuomotor mismatch.

767 (**G**) The correlation coefficient between the population activity vectors during locomotion onset (on),
768 offset (off), and during locomotion bout (btw), compared to shuffle (rnd.) controls. Here and elsewhere,
769 n.s.: not significant; *: $p<0.05$; **: $p<0.01$; ***: $p<0.001$; see **Table S1** for all statistical information.

770 (**H**) GRAB-ACh3.0 fluorescence as a function of locomotion velocity. Shown are the mean acetylcholine
771 level in each bin, corrected for hemodynamics. Shading marks SEM. We found no evidence of a difference
772 in acetylcholine level between low and high locomotion velocities (indicated by gray shading). Note, the
773 x-axis range is matched to that in **Figure 2E**. Because we had overall less data in these GRAB experiments,
774 reliable estimates of mean acetylcholine levels were not possible for locomotion velocities above
775 approximately 13 cm/s.

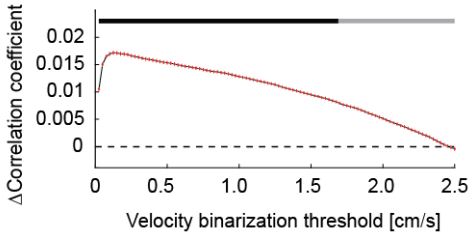

776

777 **Figure S3. Cholinergic axon activity correlated better with a binarized locomotion vector than with the**
778 **unfiltered locomotion vector over a large range of binarization thresholds. Related to Figure 2.**

779 The correlation between activity of cholinergic axons in visual cortex and locomotion velocity was higher
780 when we used a binarized version of the locomotion velocity trace. This difference was present over a
781 large range of thresholds. The black bar at the top of the plot indicates threshold values for which the
782 correlation with binarized locomotion velocity was higher than that with raw locomotion velocity.

783

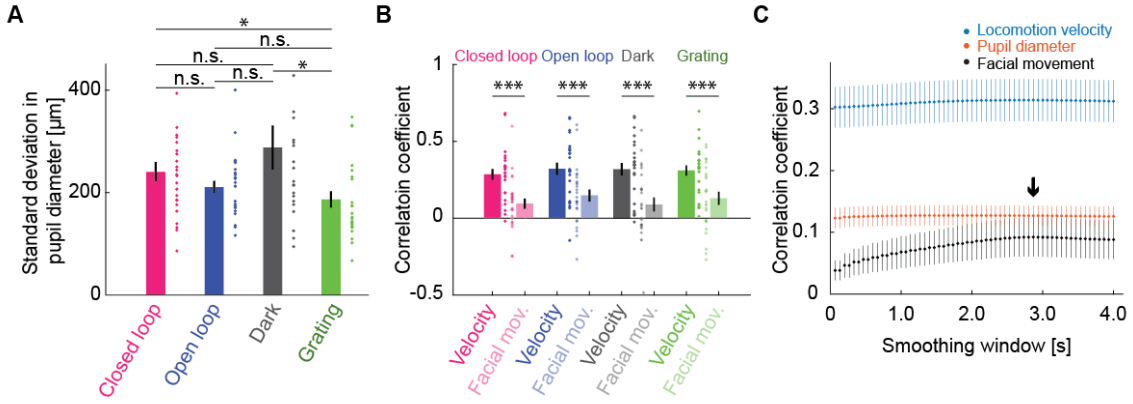

Figure S4. Activity of cholinergic axons correlated better with locomotion velocity than with facial movement. Related to Figure 3.

(**A**) Standard deviation of pupil diameter as a function of visuomotor condition. Here and elsewhere, n.s.: not significant; *: $p < 0.05$; **: $p < 0.01$; ***: $p < 0.001$; see **Table S1** for all statistical information.

(**B**) Average correlation of activity of cholinergic axons in visual cortex with facial movements as a function of visuomotor condition, compared with the same activity correlation to locomotion velocity (same data as **Figure 3A**). Error bars indicate SEM. Individual data points are imaging sites.

(**C**) Average correlation of activity of cholinergic axons in visual cortex and locomotion velocity (blue), pupil diameter (red), or facial movement (black) as a function of smoothing window. The black arrow marks the smoothing window used for facial movements.

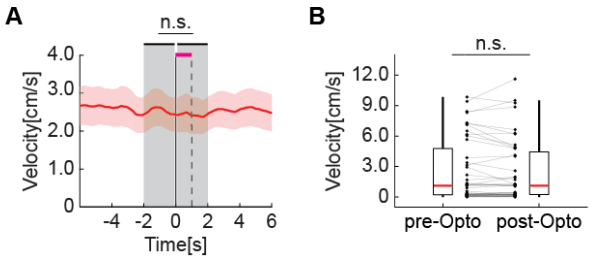

Figure S5. Optogenetic stimulation of basal forebrain cholinergic axons in visual cortex did not change the locomotion velocity of the mice. Related to Figure 4.

(**A**) Locomotion velocity before, during, and after optogenetic stimulation of cholinergic axons. Shown are the mean (red line) and SEM (red shading) across imaging sites. Here and elsewhere, n.s.: not significant; *: $p<0.05$; **: $p<0.01$; ***: $p<0.001$; see **Table S1** for all statistical information.

(**B**) Average locomotion velocity before optogenetic stimulation (-2 s to 0 s) is indistinguishable from the locomotion velocity during and immediately after stimulation (0 s to 2 s; stimulation occurs from 0 s to 1 s). Each dot is an imaging site. Boxes show 25th and 75th percentile, red line is the median, and the whiskers extend to the most extreme datapoints not considered outliers.

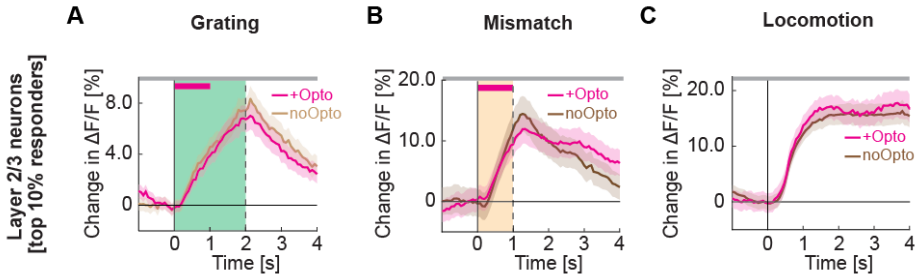

Figure S6. Optogenetic activation of cholinergic axons in visual cortex does not increase the responsiveness of the layer 2/3 neurons most responsive to gratings, visuomotor mismatch, or locomotion onset. Related to Figure 4.

(**A**) Average calcium response to full field drifting gratings of the 10 % of layer 2/3 neurons in visual cortex most responsive to full field drifting gratings while the mice were stationary, without (light brown) or with (pink) optogenetic activation of cholinergic axons in visual cortex. To avoid regression to the mean artifacts, neurons are selected based on half of the trials, and the responses of the other half of trials are shown here. Duration of the optogenetic stimulation is marked by a pink bar. Green shading indicates duration of the grating stimulus. The responses are compared bin-by-bin using a nested hierarchical bootstrap test. Here and in subsequent panels, bins with a significant difference ($p < 0.05$) are indicated by a black line above the plot; those with $p > 0.05$ are marked gray. Shading marks SEM.

(**B**) As in **A**, but for the 10 % of layer 2/3 neurons most responsive to visuomotor mismatch.

(**C**) As in **A**, but for the 10 % of layer 2/3 neurons most responsive to locomotion onset in closed loop.

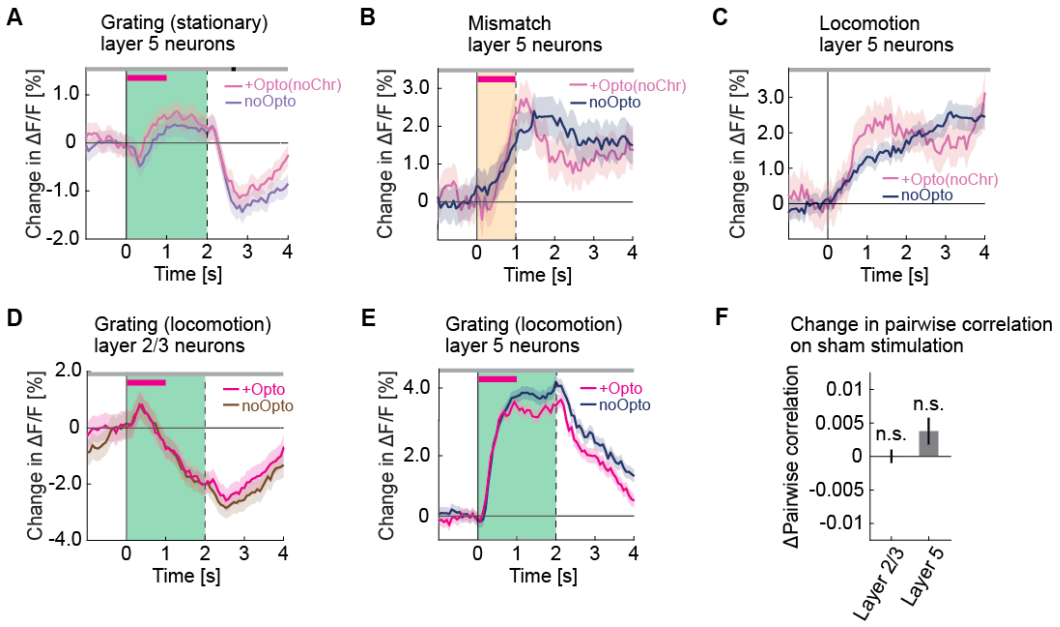

Figure S7. Optogenetic activation did not increase grating responses during locomotion and had no effect in opsin-negative control mice. Related to Figures 4 and 6.

(**A**) Average calcium response of layer 5 neurons in visual cortex to full field drifting gratings (green shading) presented while the mice were stationary, without (pale blue) and with (pale pink) optogenetic stimulation in mice that did not express ChrimsonR in cholinergic axons. The duration of stimulation is marked by a pink bar.

(**B**) Average calcium response of layer 5 neurons in visual cortex to visuomotor mismatch (orange shading) without (blue) and with (pale pink) optogenetic light stimulation in mice that do not express ChrimsonR in cholinergic axons. The duration of stimulation light is marked by a pink bar.

(**C**) As in **B**, but for locomotion onset responses. Note, the locomotion onset threshold was relaxed to 0.025 cm/s to increase the number of onsets we could analyze.

(**D**) Average calcium response of layer 2/3 neurons in visual cortex to full field drifting gratings (green shading) presented while the mice were locomoting, without (brown) and with (pink) optogenetic stimulation of cholinergic axons in visual cortex. The duration of optogenetic stimulation is marked by a pink bar. The responses are compared bin-by-bin using a nested hierarchical bootstrap test. Here and in subsequent panels, bins with a significant difference ($p < 0.05$) are indicated by a black line above the plot; those with $p > 0.05$ are marked gray. Shading marks SEM.

(**E**) As in **D**, but for layer 5 neurons.

(**F**) Change in pairwise correlations in layer 2/3 neurons and in layer 5 neurons in visual cortex during sham stimulation while the mice were stationary. Here and elsewhere, n.s.: not significant; *: $p < 0.05$; **: $p < 0.01$; ***: $p < 0.001$; see **Table S1** for all statistical information.

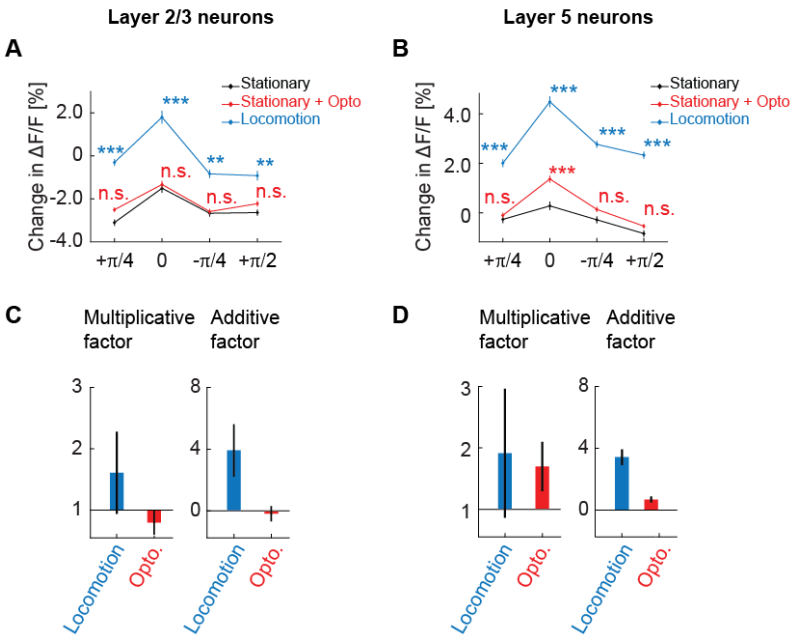

Figure S8. Cholinergic stimulation primarily has a multiplicative influence on the orientation tuning curve of layer 5 neurons. Related to Figure 4.

(**A**) Average calcium response of layer 2/3 neurons in visual cortex to different orientations of full field drifting gratings while mice were stationary (black), on optogenetic stimulation of cholinergic axons while mice were stationary (red), and while mice were locomoting (blue). Here and elsewhere, n.s.: not significant; *: $p < 0.05$; **: $p < 0.01$; ***: $p < 0.001$; see **Table S1** for all statistical information.

(**B**) As in **A**, but for layer 5 neurons in visual cortex.

(**C**) Muliplicative factor (a) and additive factor (b) of a linear fit of the form y = ax +b, for the scaling of the orientation tuning curve in layer 2/3 induced by locomotion and optogenetic stimulation of cholinergic axons. Error bars indicate the standard error of the coefficients.

(**D**) Same as in **C**, but for layer 5 neurons in visual cortex.

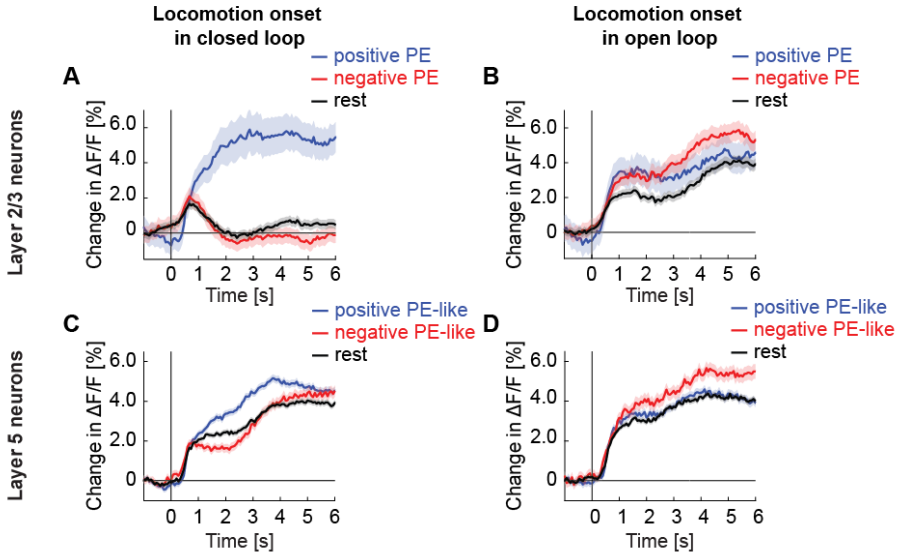

Figure S9. Locomotion onset responses are suppressed by closed loop visual feedback in layer 2/3, but not layer 5. Related to Figures 4G and 4H.

(**A**) Average calcium response of layer 2/3 neurons in visual cortex to locomotion onset in closed loop, with neurons split into positive prediction error (PE) neurons (blue), negative PE neurons (red), and the rest of the population (black). We defined the top 30% responders to grating stimuli as positive PE neurons, the top 30% responders to visuomotor mismatch as negative PE neurons, and the remaining 60% of the neurons along with any neurons that responded to both gratings and mismatch as rest.

(**B**) As in **A**, but during open loop.

(**C**) As in **A**, but for layer 5 neurons.

(**D**) As in **A**, but for layer 5 neurons in open loop.

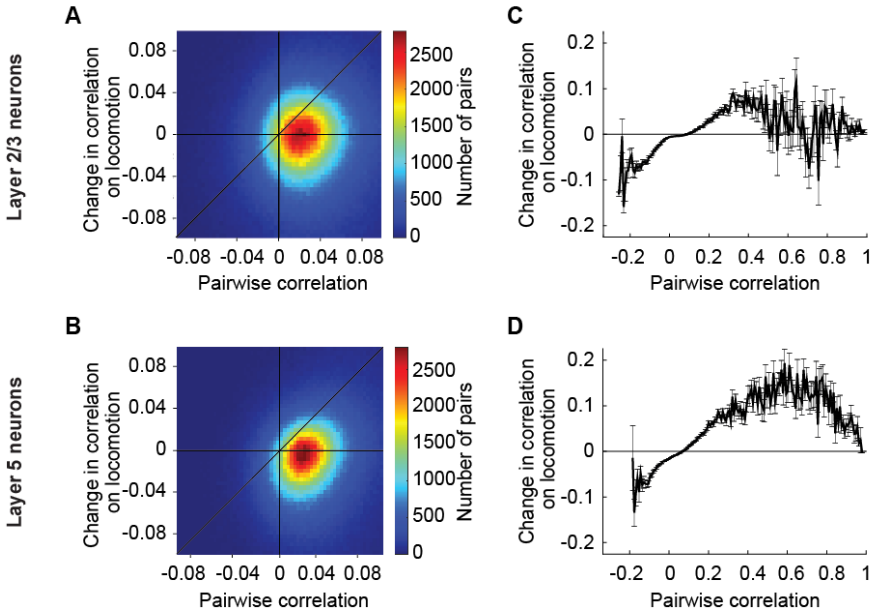

Figure S10. Locomotion increases the correlation between those layer 5 neurons in visual cortex that on average have a higher correlation. Related to Figure 6.

(**A**) Change in the pairwise correlation between pairs of layer 2/3 neurons in visual cortex on locomotion and their average correlation over the entire imaging session.

(**B**) As in **A**, but for layer 5 neurons in visual cortex.

(**C**) Related to **A,** with all neuron pairs binned by their average correlation. Bars indicate SEM.

(**D**) As in **C,** but for layer 5 neurons in visual cortex.

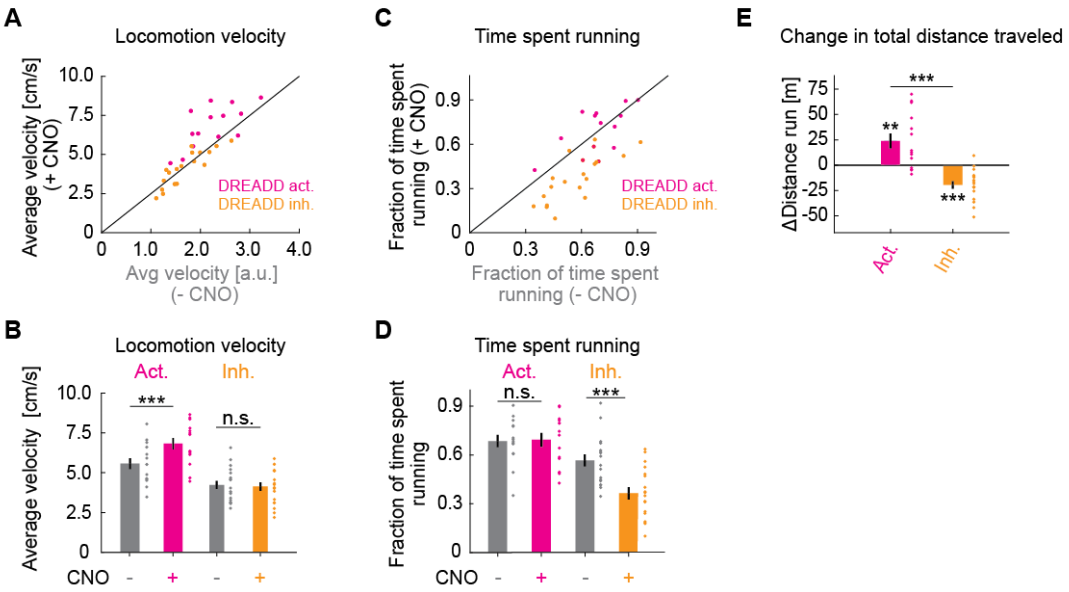

Figure S11. Chemogenetic manipulation of basal forebrain cholinergic neurons affects locomotion behavior of mice. Related to Figure 6.

(**A**) Average locomotion velocity before and after administration of CNO in ChAT-Cre mice that expressed a DREADD activator (pink) or a DREADD inhibitor (orange) in basal forebrain. Each dot is an experimental session.

(**B**) Quantification of the data shown in **A**. Here and elsewhere, n.s.: not significant; *: $p < 0.05$; **: $p < 0.01$; ***: $p < 0.001$; see **Table S1** for all statistical information.

(**C**) As in **A**, but for fraction of time spent running.

(**D**) Quantification of the data shown in **C**.

(**E**) CNO induced change in the total distance traveled.

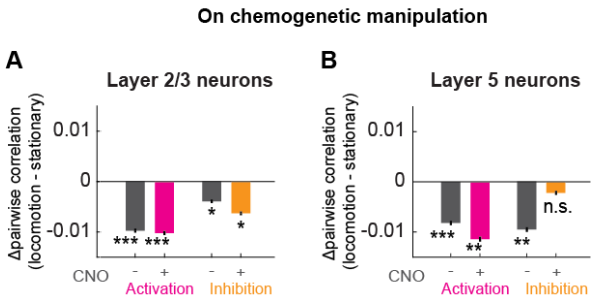

887

888 **Figure S12. Change in locomotion-related decorrelation upon chemogenetic manipulation of basal**
889 **forebrain cholinergic neurons. Related to Figure 6.**

890 (**A**) Average change in pairwise correlations of layer 2/3 neurons of visual cortex during locomotion in the
891 group of mice before (gray, left) and after (pink) DREADD activation, and in the group before (gray, right)
892 and after (orange) DREADD inhibition of basal forebrain cholinergic neurons. Here and elsewhere, n.s.:
893 not significant; *: $p < 0.05$; **: $p < 0.01$; ***: $p < 0.001$; see **Table S1** for all statistical information. Note,
894 the differences in pre-CNO locomotion driven decorrelation between the different groups of mice
895 complicate the direct comparison of the DREADD effects. To ease this comparison, we represented the
896 same data in **Figure 6G and 6H** as a difference to pre-CNO levels.

897 (**B**) As in **A**, but for layer 5 neurons of visual cortex.

898

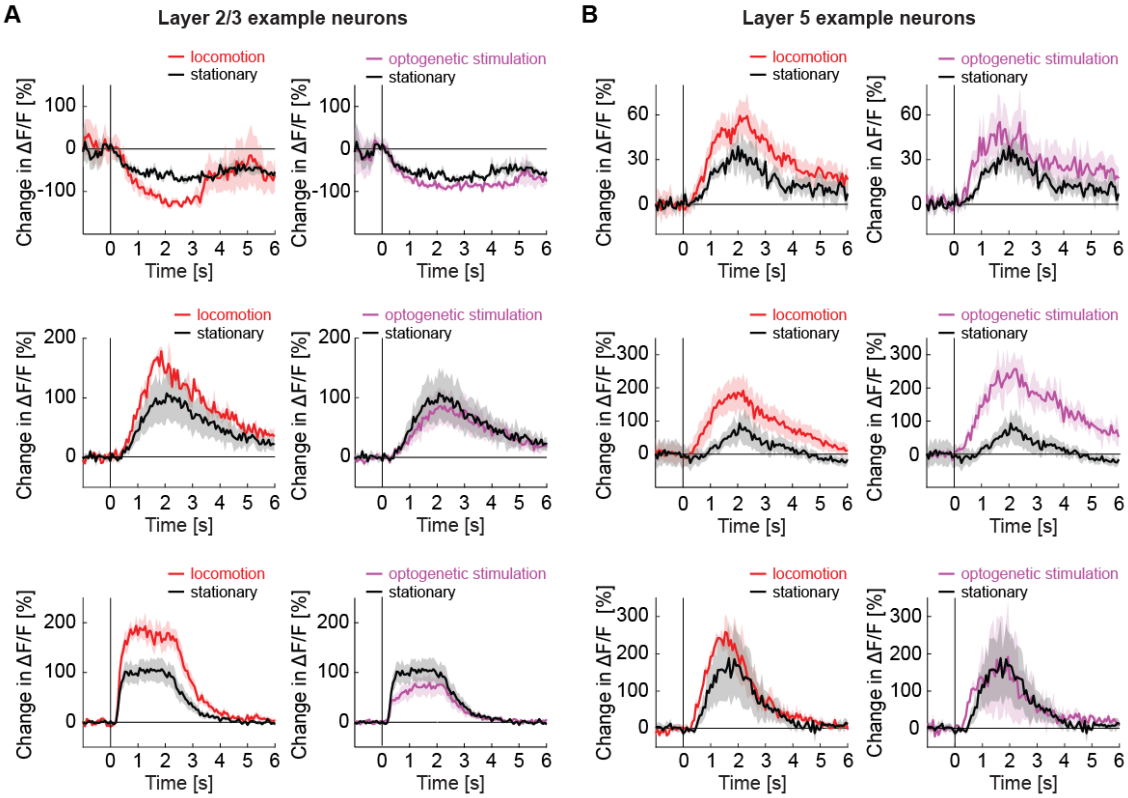

Figure S13. Locomotion and optogenetic stimulation of basal forebrain cholinergic axons decreased the latency of response to a visual stimulus in layer 5 neurons but not in layer 2/3 neurons. Related to Figure 7.

(**A**) Three example layer 2/3 neurons from visual cortex with the average response to grating stimuli in responsive trials while the mouse is stationary (black), locomoting (red), or on optogenetic stimulation of cholinergic axons in visual cortex (purple).

(B) As in **A**, but for three example layer 5 neurons.

SUPPLEMENTARY VIDEOS

Video S1. Mouse running speeds.

Mouse running on a spherical treadmill at different speeds to illustrate the range of running speeds covered by our data.

ACKNOWLEDGEMENTS

We thank all the members of the Keller lab for discussion and support. This project has received funding from the Swiss National Science Foundation (GBK), the Novartis Research Foundation (GBK), and the European Research Council (ERC) under the European Union's Horizon 2020 research and innovation programme (grant agreement No 865617) (GBK).

AUTHOR CONTRIBUTIONS

BY designed and performed the experiments and analyzed the data. All authors wrote the manuscript.

DECLARATION OF INTERESTS

The authors declare no competing financial interests.

REFERENCES

Alitto, H.J., Dan, Y., 2012. Cell-type-specific modulation of neocortical activity by basal forebrain input. Front. Syst. Neurosci. https://doi.org/10.3389/fnsys.2012.00079

Attinger, A., Wang, B., Keller, G.B., Attinger, A., Wang, B., Keller, G.B., 2017. Visuomotor coupling shapes the functional development of mouse visual cortex. Cell 169, 1291–1302. https://doi.org/10.1016/j.cell.2017.05.023

Ayaz, A., Saleem, A.B., Schölvinck, M.L., Carandini, M., 2013. Locomotion Controls Spatial Integration in Mouse Visual Cortex. Curr. Biol. 23, 890–894. https://doi.org/10.1016/J.CUB.2013.04.012

Aydın, Ç., Couto, J., Giugliano, M., Farrow, K., Bonin, V., 2018. Locomotion modulates specific functional cell types in the mouse visual thalamus. Nat. Commun. 9, 4882. https://doi.org/10.1038/s41467-018-06780-3

Bakin, JS., Weinberger, NM., Sharma, J., Perea, G., Petravicz, J., Le, C., Sur, M., 2012. Induction of a physiological memory in the cerebral cortex by stimulation of the nucleus basalis. PNAS 93, 11219–11224. https://doi.org/10.1073/pnas.93.20.11219

Bear, M.F., Singer, W., 1986. Modulation of visual cortical plasticity by acetylcholine and noradrenaline. Nature 320, 172–176. https://doi.org/10.1038/320172a0

Broussard, G.J., Liang, Y., Fridman, M., Unger, E.K., Meng, G., Xiao, X., Ji, N., Petreanu, L., Tian, L., 2018. In vivo measurement of afferent activity with axon-specific calcium imaging. Nat. Neurosci. 21. https://doi.org/10.1038/s41593-018-0211-4

Chatfield, P.O., Dempsey, E.W., 1941. Some effects of prostigmine and acetylcholine on cortical potentials [WWW Document]. URL https://journals.physiology.org/doi/abs/10.1152/ajplegacy.1942.135.3.633 (accessed 3.20.23).

Chen, N., Sugihara, H., Sur, M., 2015. An acetylcholine-activated microcircuit drives temporal dynamics of cortical activity. Nat. Neurosci. 18, 892–902. https://doi.org/10.1038/nn.4002

Colangelo, C., Shichkova, P., Keller, D., Markram, H., Ramaswamy, S., 2019. Cellular, synaptic and network effects of acetylcholine in the neocortex. Front. Neural Circuits 13. https://doi.org/10.3389/fncir.2019.00024

Collins, L., Francis, J., Emanuel, B., McCormick, D.A., 2023. Cholinergic and noradrenergic axonal activity contains a behavioral-state signal that is coordinated across the dorsal cortex. eLife 12, e81826. https://doi.org/10.7554/eLife.81826

Dadarlat, M.C., Stryker, M.P., 2017. Locomotion enhances neural encoding of visual stimuli in mouse V1. J. Neurosci. 37, 3764–3775. https://doi.org/10.1523/JNEUROSCI.2728-16.2017

Davies, P., Maloney, A.J., 1976. Selective loss of central cholinergic neurons in Alzheimer's disease. Lancet Lond. Engl. 2, 1403. https://doi.org/10.1016/s0140-6736(76)91936-x

Dombeck, D.A., Khabbaz, A.N., Collman, F., Adelman, T.L., Tank, D.W., 2007. Imaging large-scale neural activity with cellular resolution in awake, mobile mice. Neuron 56, 43–57. https://doi.org/10.1016/j.neuron.2007.08.003

Eggermann, E., Kremer, Y., Crochet, S., Petersen, C.C.H., 2014. Cholinergic Signals in Mouse Barrel Cortex during Active Whisker Sensing. Cell Rep. 9, 1654–1660. https://doi.org/10.1016/j.celrep.2014.11.005

Ego-Stengel, V., Shulz, D.E., Haidarliu, S., Sosnik, R., Ahissar, E., 2001. Acetylcholine-Dependent Induction and Expression of Functional Plasticity in the Barrel Cortex of the Adult Rat. J. Neurophysiol. 86, 422–437. https://doi.org/10.1152/jn.2001.86.1.422

Erisken, S., Vaiceliunaite, A., Jurjut, O., Fiorini, M., Katzner, S., Busse, L., 2014. Effects of Locomotion Extend throughout the Mouse Early Visual System. Curr. Biol. 24, 2899–2907. https://doi.org/10.1016/j.cub.2014.10.045

968 Forster, F.M., McCarter, R.H., 1946. The effects of local applications of acetylcholine to the acoustic cortex.
969 J. Neuropathol. Exp. Neurol. 5, 24–28. https://doi.org/10.1097/00005072-194601000-00002
970 Francis, P.T., Palmer, A.M., Snape, M., Wilcock, G.K., 1999. The cholinergic hypothesis of Alzheimer's
971 disease: a review of progress. J. Neurol. Neurosurg. Psychiatry 66, 137–147.
972 https://doi.org/10.1136/jnnp.66.2.137
973 Froemke, R.C., Merzenich, M.M., Schreiner, C.E., 2007. A synaptic memory trace for cortical receptive field
974 plasticity. Nature 450, 425–429. https://doi.org/10.1038/nature06289
975 Fu, Y., Tucciarone, J.M., Espinosa, J.S., Sheng, N., Darcy, D.P., Nicoll, R.A., Huang, Z.J., Stryker, M.P., 2014.
976 A Cortical Circuit for Gain Control by Behavioral State. Cell 156, 1139–1152.
977 https://doi.org/10.1016/j.cell.2014.01.050
978 Gasselin, C., Hohl, B., Vernet, A., Crochet, S., Petersen, C.C.H., 2021. Cell-type-specific nicotinic input
979 disinhibits mouse barrel cortex during active sensing. Neuron 109, 778-787.e3.
980 https://doi.org/10.1016/j.neuron.2020.12.018
981 Goard, M., Dan, Y., 2009. Basal forebrain activation enhances cortical coding of natural scenes. Nat.
982 Neurosci. 12, 1444–1449. https://doi.org/10.1038/nn.2402
983 Granger, A.J., Wang, W., Robertson, K., El-Rifai, M., Zanello, A.F., Bistrong, K., Saunders, A., Chow, B.W.,
984 Nuñez, V., Turrero García, M., Harwell, C.C., Gu, C., Sabatini, B.L., 2020. Cortical ChAT+ neurons
985 co-transmit acetylcholine and GABA in a target- and brain-region-specific manner. eLife 9, e57749.
986 https://doi.org/10.7554/eLife.57749
987 Greuel, J.M., Luhmann, H.J., Singer, W., 1988. Pharmacological Induction of Use-Dependent Receptive
988 Field Modifications in the Visual Cortex. Science 242, 74–77.
989 https://doi.org/10.1126/science.2902687
990 Gu, Q., Singer, W., 1993. Effects of intracortical infusion of anticholinergic drugs on neuronal plasticity in
991 kitten striate cortex. Eur. J. Neurosci. 5, 475–485. https://doi.org/10.1111/j.1460-
992 9568.1993.tb00514.x
993 Gulledge, A.T., Stuart, G.J., 2005. Cholinergic Inhibition of Neocortical Pyramidal Neurons. J. Neurosci. 25,
994 10308–10320. https://doi.org/10.1523/JNEUROSCI.2697-05.2005
995 Guo, W., Robert, B., Polley, D.B., 2019. The Cholinergic Basal Forebrain Links Auditory Stimuli with Delayed
996 Reinforcement to Support Learning. Neuron 103, 1164-1177.e6.
997 https://doi.org/10.1016/j.neuron.2019.06.024
998 Hampel, H., Mesulam, M.-M., Cuello, A.C., Khachaturian, A.S., Vergallo, A., Farlow, M.R., Snyder, P.J.,
999 Giacobini, E., Khachaturian, Z.S., 2019. Revisiting the Cholinergic Hypothesis in Alzheimer's
1000 Disease: Emerging Evidence from Translational and Clinical Research. J. Prev. Alzheimers Dis. 6,
1001 2–15. https://doi.org/10.14283/jpad.2018.43
1002 Hangya, B., Ranade, S.P., Lorenc, M., Kepecs, A., 2015. Central Cholinergic Neurons Are Rapidly Recruited
1003 by Reinforcement Feedback. Cell 162, 1155–1168. https://doi.org/10.1016/j.cell.2015.07.057
1004 Harrison, T.C., Pinto, L., Brock, J.R., Dan, Y., 2016. Calcium Imaging of Basal Forebrain Activity during Innate
1005 and Learned Behaviors. Front. Neural Circuits 10, 36. https://doi.org/10.3389/fncir.2016.00036
1006 Hay, Y.A., Lambolez, B., Tricoire, L., 2016. Nicotinic Transmission onto Layer 6 Cortical Neurons Relies on
1007 Synaptic Activation of Non-α7 Receptors. Cereb. Cortex N. Y. N 1991 26, 2549–2562.
1008 https://doi.org/10.1093/cercor/bhv085
1009 Hedrick, T., Waters, J., 2015. Acetylcholine excites neocortical pyramidal neurons via nicotinic receptors.
1010 J. Neurophysiol. 113, 2195–2209. https://doi.org/10.1152/jn.00716.2014
1011 Heindorf, M., Keller, G.B., 2022. Reduction of layer 5 mediated long-range cortical communication by
1012 antipsychotic drugs. bioRxiv 2022.01.31.478462. https://doi.org/10.1101/2022.01.31.478462
1013 Held, R., Hein, A., 1963. Movement-produced stimulation in the development of visually guided behavior.
1014 J. Comp. Physiol. Psychol. 56, 872–6.

Jing, M., Li, Yuexuan, Zeng, J., Huang, P., Skirzewski, M., Kljakic, O., Peng, W., Qian, T., Tan, K., Zou, J., Trinh, S., Wu, R., Zhang, S., Pan, S., Hires, S.A., Xu, M., Li, H., Saksida, L.M., Prado, V.F., Bussey, T.J., Prado, M.A.M., Chen, L., Cheng, H., Li, Yulong, 2020. An optimized acetylcholine sensor for monitoring in vivo cholinergic activity. Nat. Methods 17, 1139–1146. https://doi.org/10.1038/s41592-020-0953-2

Jordan, R., Keller, G.B., 2023. The locus coeruleus broadcasts prediction errors across the cortex to promote sensorimotor plasticity (preprint). elife. https://doi.org/10.7554/eLife.85111.1

Jordan, R., Keller, G.B., 2020. Opposing Influence of Top-down and Bottom-up Input on Excitatory Layer 2/3 Neurons in Mouse Primary Visual Cortex. Neuron 108, 1194-1206.e5. https://doi.org/10.1016/j.neuron.2020.09.024

Kanamaru, T., Aihara, K., 2019. Acetylcholine-mediated top-down attention improves the response to bottom-up inputs by deformation of the attractor landscape. PloS One 14, e0223592. https://doi.org/10.1371/journal.pone.0223592

Kaneko, M., Stryker, M.P., 2014. Sensory experience during locomotion promotes recovery of function in adult visual cortex. eLife 3. https://doi.org/10.7554/eLife.02798

Keller, G.B., Bonhoeffer, T., Hübener, M., 2012. Sensorimotor mismatch signals in primary visual cortex of the behaving mouse. Neuron 74, 809–15. https://doi.org/10.1016/j.neuron.2012.03.040

Keller, G.B., Mrsic-Flogel, T.D., 2018. Predictive Processing: A Canonical Cortical Computation. Neuron 100, 424–435. https://doi.org/10.1016/j.neuron.2018.10.003

Kilgard, M.P., Merzenich, M.M., 1998. Cortical map reorganization enabled by nucleus basalis activity. Science 279, 1714–1718. https://doi.org/10.1126/science.279.5357.1714

Kim, J.-H., Jung, A.-H., Jeong, D., Choi, I., Kim, K., Shin, S., Kim, S.J., Lee, S.-H., 2016. Selectivity of Neuromodulatory Projections from the Basal Forebrain and Locus Ceruleus to Primary Sensory Cortices. J. Neurosci. 36, 5314–5327. https://doi.org/10.1523/JNEUROSCI.4333-15.2016

Kirkwood, A., Rozas, C., Kirkwood, J., Perez, F., Bear, M.F., 1999. Modulation of long-term synaptic depression in visual cortex by acetylcholine and norepinephrine. J. Neurosci. 19, 1599–1609. https://doi.org/10.1523/jneurosci.19-05-01599.1999

Klapoetke, N.C., Murata, Y., Kim, S.S., Pulver, S.R., Birdsey-Benson, A., Cho, Y.K., Morimoto, T.K., Chuong, A.S., Carpenter, E.J., Tian, Z., Wang, J., Xie, Y., Yan, Z., Zhang, Y., Chow, B.Y., Surek, B., Melkonian, M., Jayaraman, V., Constantine-Paton, M., Wong, G.K.-S., Boyden, E.S., 2014. Independent optical excitation of distinct neural populations. Nat. Methods 11, 338–346. https://doi.org/10.1038/nmeth.2836

Korzhova, V., Marinković, P., Njavro, J.R., Goltstein, P.M., Sun, F., Tahirovic, S., Herms, J., Liebscher, S., 2021. Long-term dynamics of aberrant neuronal activity in awake Alzheimer's disease transgenic mice. Commun. Biol. 4, 1368. https://doi.org/10.1038/s42003-021-02884-7

Krnjević, K., Phillis, J.W., 1963. Acetylcholine-sensitive cells in the cerebral cortex. J. Physiol. 166, 296–327. https://doi.org/10.1113/jphysiol.1963.sp007106

Larsen, R.S., Turschak, E., Daigle, T., Zeng, H., Zhuang, J., Waters, J., 2018. Activation of neuromodulatory axon projections in primary visual cortex during periods of locomotion and pupil dilation. bioRxiv 502013–502013. https://doi.org/10.1101/502013

Laszlovszky, T., Schlingloff, D., Hegedüs, P., Freund, T.F., Gulyás, A., Kepecs, A., Hangya, B., 2020. Distinct synchronization, cortical coupling and behavioral function of two basal forebrain cholinergic neuron types. Nat. Neurosci. https://doi.org/10.1038/s41593-020-0648-0

Lee, A.M., Hoy, J.L., Bonci, A., Wilbrecht, L., Stryker, M.P., Niell, C.M., 2014. Identification of a Brainstem Circuit Regulating Visual Cortical State in Parallel with Locomotion. Neuron 83, 455–466. https://doi.org/10.1016/J.NEURON.2014.06.031

Leinweber, M., Ward, D.R., Sobczak, J.M., Attinger, A., Keller, G.B., 2017. A Sensorimotor Circuit in Mouse Cortex for Visual Flow Predictions. Neuron 95, 1420-1432.e5. https://doi.org/10.1016/j.neuron.2017.08.036

Leinweber, M., Zmarz, P., Buchmann, P., Argast, P., Hübener, M., Bonhoeffer, T., Keller, G.B., 2014. Two-photon calcium imaging in mice navigating a virtual reality environment. J. Vis. Exp. JoVE e50885. https://doi.org/10.3791/50885

Li, X., Yu, B., Sun, Q., Zhang, Y., Ren, M., Zhang, X., Li, A., Yuan, J., Madisen, L., Luo, Q., Zeng, H., Gong, H., Qiu, Z., 2018. Generation of a whole-brain atlas for the cholinergic system and mesoscopic projectome analysis of basal forebrain cholinergic neurons. Proc. Natl. Acad. Sci. U. S. A. 115, 415–420. https://doi.org/10.1073/pnas.1703601115

Lohani, S., Moberly, A.H., Benisty, H., Landa, B., Jing, M., Li, Y., Higley, M.J., Cardin, J.A., 2022. Spatiotemporally heterogeneous coordination of cholinergic and neocortical activity. Nat. Neurosci. 25, 1706–1713. https://doi.org/10.1038/s41593-022-01202-6

Metherate, R., Weinberger, N.M., 1990. Cholinergic modulation of responses to single tones produces tone-specific receptive field alterations in cat auditory cortex. Synapse 6, 133–145. https://doi.org/10.1002/syn.890060204

Minces, V., Pinto, L., Dan, Y., Chiba, A.A., 2017. Cholinergic shaping of neural correlations. Proc. Natl. Acad. Sci. U. S. A. 114, 5725–5730. https://doi.org/10.1073/pnas.1621493114

Nelson, A., Mooney, R., 2016. The Basal Forebrain and Motor Cortex Provide Convergent yet Distinct Movement-Related Inputs to the Auditory Cortex. Neuron 90, 635–648. https://doi.org/10.1016/j.neuron.2016.03.031

Niell, C.M., Stryker, M.P., 2010. Modulation of Visual Responses by Behavioral State in Mouse Visual Cortex. Neuron 65, 472–479. https://doi.org/10.1016/j.neuron.2010.01.033

Niell, C.M., Stryker, M.P., 2008. Highly Selective Receptive Fields in Mouse Visual Cortex. J. Neurosci. 28, 7520–7536. https://doi.org/10.1523/JNEUROSCI.0623-08.2008

Obermayer, J., Verhoog, M.B., Luchicchi, A., Mansvelder, H.D., 2017. Cholinergic modulation of cortical microcircuits is layer-specific: Evidence from rodent, monkey and human brain. Front. Neural Circuits 11. https://doi.org/10.3389/fncir.2017.00100

Pafundo, D.E., Nicholas, M.A., Zhang, R., Kuhlman, S.J., 2016. Top-Down-Mediated Facilitation in the Visual Cortex Is Gated by Subcortical Neuromodulation. J. Neurosci. 36, 2904–2914. https://doi.org/10.1523/JNEUROSCI.2909-15.2016

Pakan, J.M., Lowe, S.C., Dylda, E., Keemink, S.W., Currie, S.P., Coutts, C.A., Rochefort, N.L., 2016. Behavioral-state modulation of inhibition is context-dependent and cell type specific in mouse visual cortex. eLife 5. https://doi.org/10.7554/eLife.14985

Perry, E.K., Tomlinson, B.E., Blessed, G., Bergmann, K., Gibson, P.H., Perry, R.H., 1978. Correlation of cholinergic abnormalities with senile plaques and mental test scores in senile dementia. Br. Med. J. 2, 1457–1459.

Pinto, L., Goard, M.J., Estandian, D., Xu, M., Kwan, A.C., Lee, S.-H., Harrison, T.C., Feng, G., Dan, Y., 2013. Fast modulation of visual perception by basal forebrain cholinergic neurons. Nat. Neurosci. 2013 1612 16, 1857–1857. https://doi.org/10.1038/nn.3552

Polack, P.-O., Friedman, J., Golshani, P., 2013. Cellular mechanisms of brain state–dependent gain modulation in visual cortex. Nat. Neurosci. 16, 1331–1339. https://doi.org/10.1038/nn.3464

Rasmusson, D.D., Dykes, R.W., 1988. Long-term enhancement of evoked potentials in cat somatosensory cortex produced by co-activation of the basal forebrain and cutaneous receptors. Exp. Brain Res. 70, 276–286. https://doi.org/10.1007/BF00248353

Reimer, J., Froudarakis, E., Cadwell, C.R., Yatsenko, D., Denfield, G.H., Tolias, A.S., 2014. Pupil Fluctuations Track Fast Switching of Cortical States during Quiet Wakefulness. Neuron 84, 355–362. https://doi.org/10.1016/j.neuron.2014.09.033

Reimer, J., McGinley, M.J., Liu, Y., Rodenkirch, C., Wang, Q., McCormick, D.A., Tolias, A.S., 2016. Pupil fluctuations track rapid changes in adrenergic and cholinergic activity in cortex. Nat. Commun. https://doi.org/10.1038/ncomms13289

Ren, C., Peng, K., Yang, R., Liu, W., Liu, C., Komiyama, T., 2022. Global and subtype-specific modulation of cortical inhibitory neurons regulated by acetylcholine during motor learning. Neuron 110, 2334-2350.e8. https://doi.org/10.1016/j.neuron.2022.04.031

Robert, B., Kimchi, E.Y., Watanabe, Y., Chakoma, T., Jing, M., Li, Y., Polley, D.B., 2021. A functional topography within the cholinergic basal forebrain for encoding sensory cues and behavioral reinforcement outcomes. eLife 10, e69514. https://doi.org/10.7554/eLife.69514

Rossi, J., Balthasar, N., Olson, D., Scott, M., Berglund, E., Lee, C.E., Choi, M.J., Lauzon, D., Lowell, B.B., Elmquist, J.K., 2011. Melanocortin-4-receptors Expressed by Cholinergic Neurons Regulate Energy Balance and Glucose Homeostasis. Cell Metab. 13, 195–204. https://doi.org/10.1016/j.cmet.2011.01.010

Sachdev, R.N.S., Lu, S.-M., Wiley, R.G., Ebner, F.F., 1998. Role of the Basal Forebrain Cholinergic Projection in Somatosensory Cortical Plasticity. J. Neurophysiol. 79, 3216–3228. https://doi.org/10.1152/jn.1998.79.6.3216

Saleem, A.B., Ayaz, A., Jeffery, K.J., Harris, K.D., Carandini, M., 2013. Integration of visual motion and locomotion in mouse visual cortex. Nat. Neurosci. 16, 1864–9. https://doi.org/10.1038/nn.3567

Saravanan, V., Berman, G.J., Sober, S.J., 2020. Application of the hierarchical bootstrap to multi-level data in neuroscience. Neurons Behav. Data Anal. Theory 3, https://nbdt.scholasticahq.com/article/13927-application-of-the-hierarchical-bootstrap-to-multi-level-data-in-neuroscience.

Sato, H., Hata, Y., Masui, H., Tsumoto, T., 1987. A functional role of cholinergic innervation to neurons in the cat visual cortex. J. Neurophysiol. 58, 765–780. https://doi.org/10.1152/jn.1987.58.4.765

Sillito, A.M., Kemp, J.A., 1983. Cholinergic modulation of the functional organization of the cat visual cortex. Brain Res. 289, 143–155. https://doi.org/10.1016/0006-8993(83)90015-X

Soma, S., Shimegi, S., Suematsu, N., Tamura, H., Sato, H., 2013. Modulation-specific and laminar-dependent effects of acetylcholine on visual responses in the rat primary visual cortex. PloS One 8, e68430. https://doi.org/10.1371/journal.pone.0068430

Suzuki, M., Larkum, M.E., 2020. General Anesthesia Decouples Cortical Pyramidal Neurons. Cell 180, 666-676.e13. https://doi.org/10.1016/j.cell.2020.01.024

Terry, A.V., Buccafusco, J.J., 2003. The cholinergic hypothesis of age and Alzheimer's disease-related cognitive deficits: recent challenges and their implications for novel drug development. J. Pharmacol. Exp. Ther. 306, 821–827. https://doi.org/10.1124/jpet.102.041616

Tsuchiya, R., Yoshiki, F., Kudo, Y., Morita, M., 2002. Cell type-selective expression of green fluorescent protein and the calcium indicating protein, yellow cameleon, in rat cortical primary cultures. Brain Res. 956, 221–229. https://doi.org/10.1016/S0006-8993(02)03518-7

Unal, C.T., Golowasch, J.P., Zaborszky, L., 2012. Adult mouse basal forebrain harbors two distinct cholinergic populations defined by their electrophysiology. Front. Behav. Neurosci. 6, 21–21. https://doi.org/10.3389/fnbeh.2012.00021

Vasilevskaya, A., Widmer, F.C., Keller, G.B., Jordan, R., 2023. Locomotion-induced gain of visual responses cannot explain visuomotor mismatch responses in layer 2/3 of primary visual cortex. Cell Rep. 42, 112096. https://doi.org/10.1016/j.celrep.2023.112096

Vinck, M., Batista-Brito, R., Knoblich, U., Cardin, J.A., 2015. Arousal and Locomotion Make Distinct Contributions to Cortical Activity Patterns and Visual Encoding. Neuron 86, 740–754. https://doi.org/10.1016/j.neuron.2015.03.028

Widmer, F.C., O'Toole, S.M., Keller, G.B., 2022. NMDA receptors in visual cortex are necessary for normal visuomotor integration and skill learning. eLife 11, e71476. https://doi.org/10.7554/eLife.71476

1157 Wilson, D.A., Fletcher, M.L., Sullivan, R.M., 2004. Acetylcholine and Olfactory Perceptual Learning. Learn.
1158 Mem. 11, 28–34. https://doi.org/10.1101/lm.66404
1159 Xiang, Z., 1998. Cholinergic Switching Within Neocortical Inhibitory Networks. Science 281, 985–988.
1160 https://doi.org/10.1126/science.281.5379.985
1161 Yaguchi, M., Ohashi, Y., Tsubota, T., Sato, A., Koyano, K.W., Wang, N., Miyashita, Y., 2013. Characterization
1162 of the Properties of Seven Promoters in the Motor Cortex of Rats and Monkeys After Lentiviral
1163 Vector-Mediated Gene Transfer. Hum. Gene Ther. Methods 24, 333–344.
1164 https://doi.org/10.1089/hgtb.2012.238
1165 Zhu, F., Elnozahy, S., Lawlor, J., Kuchibhotla, K.V., 2023. The cholinergic basal forebrain provides a parallel
1166 channel for state-dependent sensory signaling to auditory cortex. Nat. Neurosci. 1–10.
1167 https://doi.org/10.1038/s41593-023-01289-5
1168 Zolles, G., Wagner, E., Lampert, A., Sutor, B., 2009. Functional expression of nicotinic acetylcholine
1169 receptors in rat neocortical layer 5 pyramidal cells. Cereb. Cortex N. Y. N 1991 19, 1079–1091.
1170 https://doi.org/10.1093/cercor/bhn158
1171